Enhanced expression of *p210BCR/ABL* and aberrant expression of *Zfp423/ZNF423* induce blast crisis of chronic myelogenous leukemia

Kazuko Miyazaki,[1] Norimasa Yamasaki,[1] Hideaki Oda,[2] Takeshi Kuwata,[3] Yohei Kanno,[4] Masaki Miyazaki,[5] Yukiko Komeno,[6] Jiro Kitaura,[6] Zen-ichiro Honda,[7] Søren Warming,[8] Nancy A. Jenkins,[9] Neal G. Copeland,[9] Toshio Kitamura,[6] Takuro Nakamura,[4] and Hiroaki Honda[1]

[1]Department of Developmental Biology, Research Institute of Radiation Biology and Medicine, Hiroshima University, Hiroshima, Japan; [2]Department of Pathology, Tokyo Women's Medical University, Tokyo, Japan; [3]Pathology Section, Clinical Laboratory Division, National Cancer Center Hospital East, Chiba, Japan; [4]Division of Carcinogenesis, The Cancer Institute of Japanese Foundation for Cancer Research, Tokyo, Japan; [5]Department of Immunology, Graduate School of Biomedical Sciences, Hiroshima University, Hiroshima, Japan; [6]Division of Cellular Therapy, The Institute of Medical Science, University of Tokyo, Tokyo, Japan; [7]Department of Allergy and Rheumatology, Graduate School of Medicine, University of Tokyo, Tokyo, Japan; [8]Department of Molecular Biology, Genentech, South San Francisco, CA; and [9]Cancer Genetics Laboratory, Institute of Molecular and Cell Biology, Singapore

Chronic myelogenous leukemia (CML) is a hematopoietic disorder originating from *p210BCR/ABL*-transformed stem cells, which begins as indolent chronic phase (CP) but progresses into fatal blast crisis (BC). To investigate molecular mechanism(s) underlying disease evolution, CML-exhibiting *p210BCR/ABL* transgenic mice were crossed with BXH2 mice that transmit a replication-competent retrovirus. Whereas nontransgenic mice in the BXH2 background exclusively developed acute myeloid leukemia, *p210BCR/ABL* transgenic littermates developed nonmyeloid leukemias, in which inverse polymerase chain reaction detected 2 common viral integration sites (CISs). Interestingly, one CIS was transgene's own promoter, which up-regulated *p210BCR/ABL* expression. The other was the 5′ noncoding region of a transcription factor, *Zfp423*, which induced aberrant *Zfp423* expression. The cooperative activities of *Zfp423* and *p210BCR/ABL* were demonstrated as follows: (1) introduction of *Zfp423* in *p210BCR/ABL* transgenic bone marrow (BM) cells increased colony-forming ability, (2) suppression of *ZNF423* (human homologue of *Zfp423*) in *ZNF423*-expressing, *p210BCR/ABL*-positive hematopoietic cells retarded cell growth, (3) mice that received a transplant of BM cells transduced with *Zfp423* and *p210BCR/ABL* developed acute leukemia, and (4) expression of *ZNF423* was found in human *BCR/ABL*-positive cell lines and CML BC samples. These results demonstrate that enhanced expression of *p210BCR/ABL* and deregulated expression of *Zfp423/ZNF423* contribute to CML BC. (Blood. 2009;113: 4702-4710)

Introduction

Chronic myelogenous leukemia (CML) is a hematopoietic disorder of multipotential stem cells, which exhibits excessive proliferation of immature and mature myeloid cells.[1,2] The cytogenetic hallmark of CML is the Ph chromosome, created by t(9;22)(q34;q11),[3] where the amino-terminal *BCR* gene on chromosome 22 is fused to most of the *ABL* proto-oncogene on chromosome 9, thereby creating an 8.5-kb *BCR/ABL* chimeric mRNA encoding a 210-kDa hybrid protein (p210BCR/ABL).[4-6] p210BCR/ABL possesses a much higher kinase activity in comparison with the normal 145-kDa c-ABL,[7] which is believed to play a critical role in the pathogenesis of the disease.

The clinical course of CML is characterized by hematologically and temporally distinct stages.[1,2] In the initial stage, called chronic phase (CP), the disease is indolent and the leukemic cells retain an ability to differentiate into mature granulocytes. After several years' duration of the chronic phase, however, the disease inevitably accelerates and ultimately progresses to the terminal fatal stage, called blast crisis (BC), which involves aggressive proliferation of immature blast cells. The frequent appearances of additional chromosomal abnormalities in the blast phase strongly suggest that superimposed genetic events would account for the disease evolution,[8] but the underlying molecular mechanism(s) has remained largely unknown.

To understand the complex processes involved in the clinical course of human CML, it is necessary to develop animal models that express *p210BCR/ABL* and recapitulate the clinical features of the disease. Major attempts have been focused on bone marrow transplantation (BMT) experiments. Mice that have been lethally irradiated and received a transplant of bone marrow (BM) cells infected with *p210BCR/ABL*-expressing retroviruses exhibited a CML-like myeloproliferative disorder.[9-11] On the other hand, generation of transgenic mice expressing *p210BCR/ABL* under various promoters also provides useful models.[12-17] We generated *p210BCR/ABL* transgenic mice using the promoter from the mouse *TEC* gene, a gene encoding protein-tyrosine kinase preferentially expressed in hematopoietic progenitor cells.[18,19] Although the founder mouse died of T-cell acute lymphoblastic leukemia (ALL) with a short latency, transgenic offspring reproducibly exhibited a myeloproliferative disorder after a long latency period.[14] Peripheral blood smear showed remarkable myeloid hyperplasia with maturation, the BM was hypercellular with a predominance of myeloid cells at various stages of differentiation, and the spleen was enlarged with proliferation and expansion of myeloid cells.[14] These

Submitted May 3, 2007; accepted January 29, 2009. Prepublished online as *Blood* First Edition paper, February 20, 2009; DOI 10.1182/blood-2007-05-088724.

The online version of this article contains a data supplement.

The publication costs of this article were defrayed in part by page charge payment. Therefore, and solely to indicate this fact, this article is hereby marked "advertisement" in accordance with 18 USC section 1734.

pictures represent cardinal features of human CML, allowing us to consider these transgenic mice an animal model for CML.

To examine whether this transgenic model is applicable for investigating pathogenic processes from CP to BC of CML, we crossed *p210BCR/ABL* transgenic mice with mice heterozygous for *p53*, a gene frequently inactivated in CML BC, and generated mice transgenic for *p210BCR/ABL* and heterozygous for *p53*.[20] Interestingly, *p210BCR/ABL* transgenic, *p53* heterozygous mice died of acute leukemia with a short latency, and the analysis of *p53* status revealed that the residual normal *p53* allele was frequently and preferentially lost in the tumor tissues.[20] In addition, we crossed *p210BCR/ABL* transgenic mice with *Dok-1/Dok-2* knockout mice and showed that the absence of Dok-1 and Dok-2 accelerated the disease phenotype and caused BC, defining the role of Dok-1 and Dok-2 in tumor suppression.[21] Based on these results, our transgenic mice can be regarded as a useful model for investigating molecular mechanism(s) underlying the progression from CP to BC of human CML.

In this report, to identify genes whose altered expression causes CML BC, *p210BCR/ABL* transgenic mice were subjected to retroviral insertional mutagenesis, by backcrossing to BXH2 mice, a recombinant inbred mouse strain that develop myeloid leukemia mainly due to a horizontally transmitted replication-competent retrovirus and intrinsic myeloid tropism induced by a mutation in the *Icsbp1/Irf8* locus.[22-24]

Methods

Mice

p210BCR/ABL transgenic mice were generated as described.[14] To allow for retroviral insertional mutagenesis, *p210BCR/ABL* transgenic males were backcrossed 4 generations to BXH2 females, because the ecotropic retrovirus in the BXH2 strain is transmitted to the progeny through the milk. Genotyping of the mice was carried out as described.[14] All the mice used in this study were kept according to the guidelines of the Institute of Laboratory Animal Science, Hiroshima University, and all murine studies were approved by the animal care committee at the Japanese Foundation for Cancer Research.

Hematologic and pathologic analyses

Peripheral blood counts were routinely examined. Smears and stamp specimens of leukemic tissues were stained with Wright-Giemsa (WG). Tissues from dead or moribund animals were fixed in 10% buffered formaldehyde and examined by light microscopy. All organs were examined grossly and representative slices were prepared for hematoxylin-eosin staining.

Southern and Northern blot analyses

To detect gene rearrangements, genomic DNAs were digested with appropriate restriction enzymes and blotted with a genomic fragment adjacent to the integration site. For transgene promoter, a *BglI-SmaI* fragment in the promoter region was used as a probe, and for *Zfp423*, a genomic fragment generated by polymerase chain reaction (PCR) (primer sequences are 5′-GTGCGCACGTTTGTGAGGAGCTATA-3′ and 5′-CCAGCTATTCTGTCCAGGAGCAAGA-3′), which corresponds to a part of the first intron, was used as a probe. To detect RNA expression, total RNA extracted using TRIzol (Invitrogen, Carlsbad, CA) or mRNA purified using Oligo-Tex (Takara Bio, Tokyo, Japan) was blotted with *p210BCR/ABL* cDNA, *Zfp423* cDNA, or a part of coding region of *ZNF423* cDNA generated by genomic PCR (primer sequences are 5′-CAACCAGAAACACAAGTGCCCCATG-3′ and 5′-GTTGCAGTGGAAGGCAGAGATGTTG-3′).

RT-PCR

RNA was extracted using TRI zol. Reverse-transcription (RT)–PCR was performed as described (primer sequences are 5′-GAATGTCATCGTCCACTCAGCC-3′ and 5′-GGCCACAAAATCATACAGTGCA-3′ for *p210BCR/ABL*, 5′-GAGGATACCCCTACGACGTG-3′ and 5′-GACTTGTCACGCTGTTCCTGTC-3′ for *Zfp423*, and 5′-GGCATCAACCACGAGTGTAAGC-3′ and 5′-CTTCTGCGGAGAGGTGTCCTGT-3′ for *ZNF423*).[25]

Western blot analysis

Proteins extraction and Western blot were performed as described.[14]

Flow cytometric analysis

Cells were stained with monoclonal antibodies and second reagents. FITC-, PE-, and biotin-labeled monoclonal antibodies were purchased from BD PharMingen (San Diego, CA; Thy-1.2, CD19, CD45R/B220, Mac-1, Gr-1, and CD3) or from eBioscience (San Diego, CA; CD43, IgM, BP-1, and CD20). Biotinylated antibodies were revealed with streptavidin-APC (BD PharMingen). Clone 2.4G2 anti-CD32:CD16 was used to block Fc receptors. Fluorescence-activated cell sorter (FACS) analysis was performed on a FACSCalibur flow cytometer (Becton Dickinson, Franklin Lakes, NJ), and the data were analyzed with FlowJo software (TreeStar, Ashland, OR).

Identification of retroviral integration sites

Genomic DNAs were digested with restriction enzymes, self-ligated, and subjected to inverse PCR as described,[22] except that the CUA and CAU repeats were deleted from the secondary PCR primers. The position mapping on the mouse chromosome was done by BLAST searching using the University of Colombo School of Computing (UCSC) Genome Bioinformatics database (http://genome.ucsc.edu/)[26] and the definition of a common integration site (CIS) was the same as in the mouse retrovirus tagged cancer gene database (RTCGD; http://rtcgd.abcc.ncifcrf.gov/).[23,27]

Retrovirus-mediated gene transfer, colony formation assay, and bone marrow transplantation

Retroviral preparation and retrovirus-mediated gene transfer were performed as described.[28] For colony assay, BM cells of 5-fluorouracil (5FU)–treated transgenic or nontransgenic littermates were cultured in αMEM plus 20% FCS supplemented with 10 ng/mL IL-6, 10 ng/mL IL-3, and 100 ng/mL SCF (R&D Systems, Minneapolis, MN). Retrovirus was generated using plat-E cells[29] and added into the medium containing BM cells with 6 mg/mL polybrene (Sigma-Aldrich, St Louis, MO), and retrovirus-infected BM cells were subjected to B-cell colony assay using MethoCult M3630 (StemCell Technologies, Vancouver, BC) that contains rhIL7. After 7 to 12 days' incubation, green colony numbers were counted under a fluorescent microscope.

For BM transplantation, BM cells extracted from 5FU-untreated Balb/c mice were cultured for 24 hours in IMDM plus 15% FCS supplemented with 10 ng/mL IL-6, 10 ng/mL IL-3, 100 ng/mL SCF, and 10 ng/mL IL-7 (R&D Systems). Retrovirus infection and BM transplantation were performed as described.[30]

Retrovirus-mediated transduction of shRNA for *ZNF423*

Two short hairpin RNA (shRNA) target sequences for *ZNF423* (5′-GACATACCAGTGCATCAAG-3′ for *shRNA*-1 and 5′-CTGTAAGTTCTGCAGCAAG-3′ for *shRNA*-2) were chosen according to the siRNA Hairpin Oligonucleotide Sequence Designer (Clontech, Mountain View, CA). Annealed double-strand oligonucleotides were subcloned into RNA-ready pSIREN-retroQ retroviral expression vector (Clontech). Human hematopoietic cells were first transduced with ecotropic retrovirus receptor (EcoRVR) to render these cells competent for ecotropic retrovirus infection.[31] Plat-E cells were then transfected with a pSIREN-retroQ vector harboring *shRNA* and the culture supernatant was used for infecting the ecotropic retrovirus to EcoRVR-expressing cells using Viro Mag (OZ Biosciences, Marseille, France). These procedures routinely yielded a high

infection efficiency (~ 60%) as judged by GFP fluorescence (not shown). Infected cells were selected with puromycin (0.4 mg/mL) for 2 weeks, subsequently cultured in puromycin-free medium for at least another 2 weeks, and subjected to Northern blot and cell proliferation assay.

Cell proliferation assay

On day 1, 10^5 cells of the parental and *shRNA*-transduced sublines were plated in a 10-cm^2 dish and cultured in RPMI plus 10% FCS. Cell numbers were counted on day 3 and day 5.

Cell lines and patient samples

Ph-positive and Ph-negative human hematopoietic cell lines were kindly provided by Drs Hiroya Aso (Hiroshima, Japan) and Toshiya Inaba (Hiroshima, Japan). Patient samples were taken after informed consent was obtained in accordance with the Declaration of Helsinki and approval from the institutional review board at Hiroshima University was granted.[32] Diagnosis of CML CP or CML BC (myeloid or B-lymphoid lineage) was performed based on morphologic, cytogenetic, immunophenotypic, and molecular analyses.

Results

Acute leukemias in *p210BCR/ABL* transgenic mice on a BXH2 background

To identify gene(s) whose alteration by retrovirus insertion contributes to blast crisis of CML, *p210BCR/ABL* transgenic mice were backcrossed to BXH2 mice that contain and transmit a replication-competent retrovirus. *p210BCR/ABL* transgenic and wild-type (nontransgenic) littermates from the N4 BXH2 backcross generation were used for this study (designated as p210BCR/ABL/BXH2 and WT/BXH2, respectively).

WT/BXH2 mice began to develop acute leukemia at 6 months after birth (Figure 1A thin continuous line). Macroscopically, the leukemic mice exhibited hepatosplenomegaly and lymph node (LN) swelling, which were occasionally associated with thymic enlargement. Pathologic analysis showed that leukemic cells having morphology of myeloblasts proliferated in the peripheral blood and infiltrated into the liver, spleen, LNs, and other tissues (data not shown). Flow cytometric analysis of the leukemic tissues showed that the blast cells were exclusively positive for Mac-1 and Gr-1 but negative for Thy1.2 and CD19, indicating that they all were of myeloid origin (data not shown).

In contrast to the WT/BXH2 mice, several p210BCR/ABL/BXH2 mice (named as nos. 30, 1, 17, 5, 18, and 23; Figure 1A thick continuous line) developed nonmyeloid leukemias with a shorter latency. Among them, 4 mice (nos. 30, 17, 18, and 23) displayed splenomegaly and LN swelling but did not show apparent hepatomegaly. The other 2 mice (nos. 1 and 5) exhibited massive thymic enlargement with pleural effusion and splenomegaly. Pathologic analysis showed that leukemic cells having morphology of lymphoblasts were evident in the peripheral blood and infiltration of the blast cells was observed in the LNs, liver, and other tissues examined (Figure 1B and not shown). Flow cytometric analysis revealed that the leukemic cells of the former 4 mice (nos. 30, 17, 18, and 23) were positive for CD19 but negative for Thy1.2, Mac-1, and Gr-1, and those of the latter 2 mice (nos. 1 and 5) were positive for Thy1.2 but negative for CD19, Mac-1, and Gr-1, indicating that they were of B-lymphoid and T-lymphoid origins, respectively (Figure 1C and not shown). Three $CD19^+$ samples (nos. 17, 18, and 30) were further analyzed with antibodies against CD20, B220, BP-1, CD43, and IgM to investigate the differentiation stages (pro-B, pre-B, or mature B). As shown in Figure S1 (available on the *Blood* website; see the Supplemental Materials link at the top of the online article), all the samples were positive for CD20, B220, BP-1, and CD43 but negative for IgM, indicating that they were pre–B-cell leukemias.

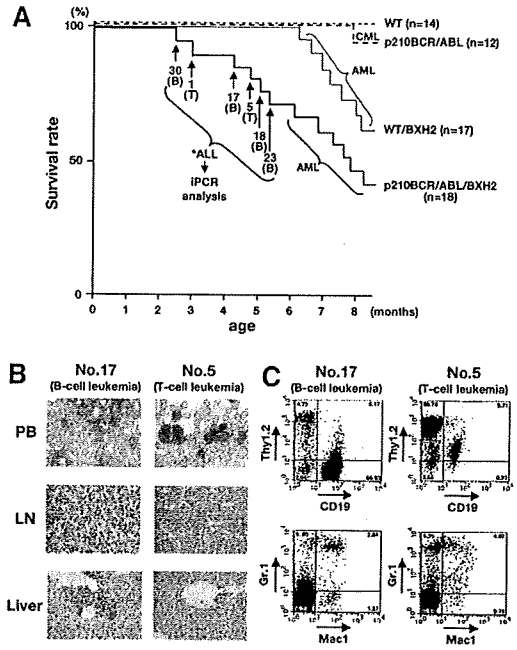

Figure 1. Survival curves and pathologic and flow cytometric analyses of leukemic mice. (A) Survival curves of the mice. The survival curves of WT/BXH2 and p210BCR/ABL/BXH2 are shown by thin and thick continuous lines, respectively, whereas those of BXH2-nonbackcrossed WT and p210BCR/ABL are shown by thin and thick dotted lines, respectively. As for the 6 p210BCR/ABL/BXH2 animals that died in a short latency and exhibited nonmyeloid phenotypes (nos. 30, 1, 17, 5, 18, and 23), the death points are indicated by → and the immunophenotypes of the disease are shown in the parentheses. T indicates T-cell leukemia; and B, B-cell leukemia. (B) Pathologic analysis of the leukemic mice. WG-stained peripheral blood smears (PB) and HE-stained lymph node (LN) and liver slices of a representative mouse for B-cell leukemia (no. 17) or T-cell leukemia (no. 5) are shown. PB smears show proliferation of blast cells and LN specimen shows the destruction of the basal structure by blast cell infiltration. In the liver, blast cells are observed around the vessel and in the sinusoids. (C) Flow cytometric analysis of mice that developed B-cell or T-cell leukemia. Blast cells of no. 17 were positive for CD19 but negative for Thy1.2, Mac-1, and Gr-1 and those of no. 5 were positive for Thy1.2 but negative for CD19, Mac-1, and Gr-1, indicating that they were of B- and T-lymphoid origins, respectively. The percentages of positive cells in each quadrant are shown.

The characteristics of the 6 p210BCR/ABL/BXH2 leukemic mice with an early disease onset are summarized in Table 1. As for the leukemias developed in the remaining p210BCR/ABL/BXH2 mice after 6 months of age, macroscopic appearances and the results of flow cytometric analysis were indistinguishable from those of the WT/BXH2 mice (data not shown). During the observation period, no mice developed hematologic disease in BXH2-nonbackcrossed WT mice and one mouse died of CML in BXH2-nonbackcrossed *p210BCR/ABL* transgenic mice (Figure 1A thin and thick dotted lines, respectively).

Enhanced expression of *p210BCR/ABL* and aberrant expression of *Zfp423* in the leukemic tissues with B-cell phenotype

We focused on the 6 p210BCR/ABL/BXH2 mice that developed nonmyeloid leukemias in a shortened period, because diseases in these mice would not be only due to the BXH2 background-derived intrinsic mechanism but caused by cooperation of *p210BCR/ABL*

Table 1. Characteristics of p210BCR/ABL/BHX2 mice with lymphoid leukemias

Mouse no.	Age at disease, mo	PB parameters			Macroscopic tumor sites	Surface markers	Diagnosis
		WBC, $\times 10^{9}$/L	Hb, g/L	Plt, $\times 10^{9}$/L			
30	2.6	11.2 (blast ~ 70%)	140	452	Spl, LN	Thy1.2$^-$, CD19$^+$, Gr.1$^-$, Mac1$^-$	B-cell leukemia
1	3.0	10.0 (blast ~ 60%)	124	238	Thy, Spl	Thy1.2$^+$, CD19$^-$, Gr.1$^-$, Mac1$^-$	T-cell leukemia
17	4.2	82.4 (blast ~ 100%)	109	525	Spl, LN	Thy1.2$^+$, CD19$^-$, Gr.1$^-$, Mac1$^-$	B-cell leukemia
5	4.8	22.0 (blast ~ 100%)	123	339	Thy, Spl, LN	Thy1.2$^-$, CD19$^+$, Gr.1$^-$, Mac1$^-$	T-cell leukemia
18	5.2	68.0 (blast ~ 100%)	118	345	Spl, LN	Thy1.2$^-$, CD19$^+$, Gr.1$^-$, Mac1$^-$	B-cell leukemia
23	5.4	19.8 (blast ~ 100%)	107	338	Spl, LN	Thy1.2$^-$, CD19$^+$, Gr.1$^-$, Mac1$^-$	B-cell leukemia

Spl indicates spleen; LN, lymph node; and Thy, thymus.

with retrovirus-inserted altered gene expression. To identify virus-affected genes in these mice, inverse PCR (iPCR) was performed and sequences of PCR fragments were subjected to BLAST searching using the UCSC Genome Bioinformatics database. Among candidate genes (listed in Table S1), we found 2 common integration sites (CISs) in B-lineage leukemias (shown by asterisks and in boldface in Table S1).

The first one was the promoter region of the mouse *TEC* gene. This CIS was found in nos. 17 and 30 and the viral integration sites were approximately 1.5-kb and approximately 200-bp upstream of the transcription initiation site,[19] respectively. Interestingly, in both cases, sequencing of the entire PCR fragment revealed that the mouse *TEC* promoter sequences were interrupted at +22 from the transcription initiation site and followed by human *BCR/ABL* cDNA. This result indicated that the integration sites were not in the endogenous mouse *TEC* gene but in the promoter region of the transgene itself. Another CIS observed in nos. 18 and 23 was in the noncoding region of the first exon of mouse *Zfp423* (*Zinc finger protein 423,* also known as *Early B-cell factor-associated zinc-finger protein, Ebfaz*) gene.[33] In these cases, the retroviruses were integrated almost in the same position, approximately 100-bp upstream of the translational initiation ATG.[33] The schematic models of the integration sites are shown in Figure 2A.

To confirm that these CISs were major integration sites in the leukemic samples, Southern blot was performed using a genomic DNA fragment adjacent to the integration site. DNA extracted from a spleen of a BXH2-nonbackcrossed *p210BCR/ABL* transgenic mouse was used as a negative control. As shown in Figure 2B, a rearranged band is evident in each sample (indicated by an arrowhead in Figure 2B), indicating that tumor cells with the CISs were predominant in the related tumors and were clonal in origin. The clonality and B-cell commitment of the leukemic cells in these mice (nos. 17, 30, 18, and 23) were further demonstrated by Southern blot using a mouse JH probe (Figure S2).

To investigate the alteration in gene expression of *p210BCR/ABL* and *Zfp423* by virus integration, RNAs extracted from tumor tissues of the 4 leukemic mice were blotted with *p210BCR/ABL* cDNA or mouse *Zfp423* cDNA. RNA extracted from a spleen of a BXH2-nonbackcrossed *p210BCR/ABL* transgenic mouse was used as control. The results are shown in upper panels of Figure 2C.

As for *p210BCR/ABL,* it is not surprising that the *p210BCR/ABL* message was not detected in the control transgenic mouse spleen (Figure 2C top left panel, "C"), because our previous data showed that the basal transgene expression was quite low, probably due to the nature of the promoter used (Honda et al[14] and data not shown). In contrast, a clear *p210BCR/ABL* message was evident in the tumors of nos. 17 and 30 (~ 7 kb, Figure 2C top left top panel, arrow). The quantitative *p210BCR/ABL* mRNA expression in these samples is shown in Figure S3. As expected from the result of the Northern blot (Figure 2C top left panel), the *p210BCR/ABL* mRNA in the control transgenic spleen was quite low and was significantly enhanced by the transgene integration (nos. 17 and 30). The enhanced expression of p210BCR/ABL at the protein level was confirmed by Western blot using an anti-ABL antibody (Figure 2C bottom left panel).

As for *Zfp423,* no clear message was observed in the control transgenic spleen (Figure 2C top right panel, "C"), which is in accordance with our previous report showing that *Zfp423* message was barely detectable in the spleen when using polyA$^+$ RNA.[34] In contrast, in nos. 18 and 23, an enhanced expression of the *Zfp423* message was observed (~ 6 kb, Figure 2C top right panel, arrow). These results indicated that the retrovirus integrations up-regulated *p210BCR/ABL* expression and induced aberrant *Zfp423* expression.

Expression of *Zfp423* in transgenic BM cells enhanced B-cell colony-forming ability, and suppression of *ZNF423* in *ZNF423*-expressing, *p210BCR/ABL*-positive CML BC cells retarded cell growth

We next investigated the effect of up-regulation and down-regulation of *Zfp423* on the proliferative ability of *p210BCR/ABL*-positive cells. We first examined whether introduction of *Zfp423* confers a growth advantage to transgenic BM cells by a colony formation assay. BM cells purified from wild-type (WT) or *p210BCR/ABL* transgenic mice were infected with control *pMysIG* or *Flag-HA*–tagged *Zfp423 (FHZfp423)*–expressing *pMysIG (pMysIG/FHZfp423)* retrovirus, and the infected cells were cultured in methylcellulose-based media (Figure 3A). Because mice with *Zfp423* activation (nos. 18 and 23) developed B-lineage leukemia, the virus-infected cells were subjected to a B-cell colony assay, and as the retrovirus vector contains *GFP* as a detection marker, colonies with green fluorescence were counted.

The results are shown in Figure 3B. No obvious difference in the colony numbers was found between control *pMysIG* virus-infected WT (WT+control) and *p210BCR/ABL* transgenic (p210BCR/ABL+control) BM cells. This result indicates that the basal *p210BCR/ABL* expression in this transgenic system does not affect the proliferative ability of B cells, probably due to the nature of the promoter used, and is in accordance with our observation that the *p210BCR/ABL* transgenic mice have not developed B-cell disease so far.[14] *pMysIG/FHZfp423*-infected WT BM cells (WT+FHZfp423) showed a slight increase in the colony number in this system. In contrast, *pMysIG/FHZfp423*-infected *p210BCR/ABL* transgenic BM cells (p210BCR/ABL+FHZfp423) generated a significantly increased number of colonies.

We next tried to down-regulate endogenous *ZNF423* (the human homologue of *Zfp423*) by RNA interference and examined its effect on the growth rate. We designed 2 short hairpin RNAs targeted to *ZNF423* mRNA (*shRNA*-1 and *shRNA*-2) and introduced them into BV-173, a *p210BCR/ABL*-positive and *ZNF423*-expressing human hematopoietic cell line (see Figure 5A). As shown in Figure 3C, introduction of *shRNA*-1 effectively decreased

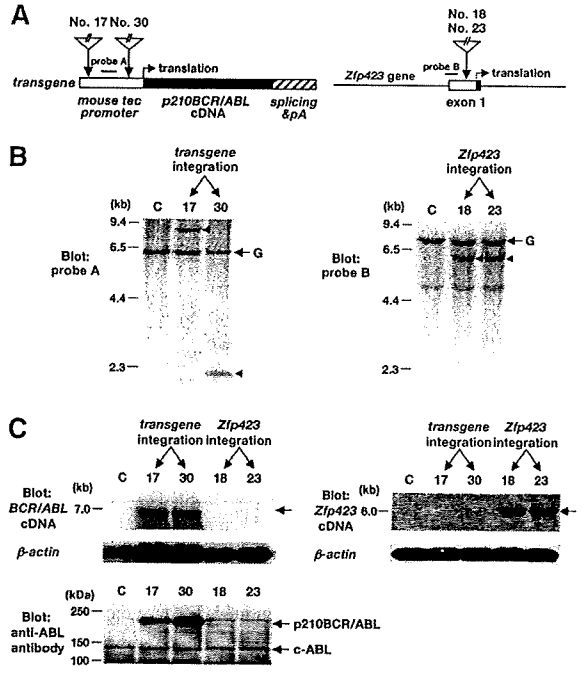

Figure 2. Retrovirus integration sites, genomic rearrangements, and altered gene expressions in mice with B-cell leukemia. (A) Schematic models of retrovirus integration sites. The retrovirus integration sites are indicated by vertical arrows. The left panel illustrates the transgene structure, where the mouse *TEC* promoter, *p210BCR/ABL* cDNA, and polyA and splicing signals are shown by dotted, filled, and shaded boxes, respectively. In mice nos. 17 and 30, retroviruses were integrated approximately 1.5-kb and approximately 200-bp upstream of the transcriptional initiation site, respectively. In the right panel, the noncoding and coding regions of *Zfp423* exon 1 are shown by blank and filled boxes, respectively. In mice nos. 18 and 23, the viral integration occurred almost in the same site, approximately 100-bp upstream of the translational initiation site. The positions of probes used for Southern blots are also shown. (B) Southern blots to confirm the CISs as major integration sites. Genomic DNAs extracted from the spleen of a control transgenic mouse (C) and tumor tissues of the diseased mice (nos. 17, 30, 18, and 23) were digested with *Bam*HI and blotted with a DNA fragment adjacent to the integration site. Probe A (A) was used for transgene rearrangement (nos. 17 and 30, left panel) and probe B was used for *Zfp423* gene rearrangement (nos. 18 and 23, right panel). The positions of germline (G) and rearranged bands are indicated by → and ◄, respectively. Molecular markers are shown on the left. (C) Enhanced expression of *p210BCR/ABL* in mice nos. 17 and 30 and up-regulated expression of *Zfp423* in mice nos. 18 and 23. For detecting *p210BCR/ABL* message, 20 μg total RNAs extracted from the spleen of a control *p210BCR/ABL* transgenic mouse (C) and tumor tissues of the diseased mice (nos. 17, 30, 18, and 23) were blotted with *p210BCR/ABL* cDNA (top left panel) and for detecting *Zfp423* message, 3 μg mRNAs from the same tissues were blotted with a part of *Zfp423* cDNA (top right panel). The result of β-*actin* hybridization is shown as an internal control. Molecular markers are shown on the left and the positions of *p210BCR/ABL* and *Zfp423* messages are indicated by →. Enhanced expression of p210BCR/ABL protein in mice nos. 17 and 30 was detected by blotting the proteins extracted from the same tissues with an anti-ABL antibody (bottom left panel). Protein markers are shown on the left and the positions of p210BCR/ABL and c-ABL (145 kDa) are indicated by →.

ZNF423 mRNA to approximately 40% of that in the parental cells, whereas *shRNA*-2 was less effective. Concurrently, as shown Figure 3D, BV-173 cells transduced with *shRNA*-1 displayed a significantly reduced growth rate, whereas cells expressing *shRNA*-2 showed only marginal growth retardation. To confirm that the *shRNA*s did not affect the growth of cells without *ZNF423* expression, the same *shRNA*s were introduced into KOPN67, a *p210BCR/ABL*-positive but *ZNF423*-nonexpressing cell line (see Figure 5A). As expected, no difference in cell growth was observed in the parental line and *shRNA*s-transduced sublines (Figure S4), confirming the specificity of the *shRNA*s on the *ZNF423*-dependent cell growth. These results indicated that *Zfp423/ZNF423* cooperated with *p210BCR/ABL* and enhanced proliferation of *p210BCR/ABL*-expressing hematopoietic cells.

Zfp423 accelerated disease onset of *p210BCR/ABL*-induced leukemia and increased incidence of B-ALL

We then investigated the in vivo cooperative activity of *Zfp423* and *p210BCR/ABL* by a BMT approach. Because *p210BCR/ABL* transgenic mice were not congenic enough for BMT, we generated *p210BCR/ABL*-expressing retrovirus and *FHZfp423*-expressing retrovirus separately, and infected them with BM cells of Balb/c mice, the strain that has been successfully used to develop CML in the BMT experiments.[10,11] And because *Zfp423*-positive leukemias (nos. 18 and 23) were of B-cell phenotype, BM cells were not pretreated with 5FU and in vitro cultures were performed using a cytokine cocktail with IL-6, IL-3, SCF, and IL-7, as previously described.[11]

BM cells infected with control retrovirus, *p210BCR/ABL*-expressing retrovirus, *FHZfp423*-expressing retrovirus, or both types of viruses were transplanted into sublethally irradiated syngeneic mice (Figure 4A). To detect *p210BCR/ABL*- and *FHZfp423*-positive cells by flow cytometry, cells expressing *p210BCR/ABL* and *FHZfp423* were labeled with *GFP* and *KO* (*Kusabira Orange*),[35] respectively (Figure 4A). The protein expression of the inserted cDNA by retrovirus infection was confirmed by Western blot (Figure S5).

The mice that underwent transplantation were continuously observed and peripheral blood parameters were routinely examined for morphologic changes by Wight-Giemsa staining and for *GFP* and/or *KO* positivities by flow cytometry. The survival rate of each group evaluated using the Kaplan-Meier test is shown in the upper panel of Figure 4B. No disease developed in the control virus-transduced mice. In addition, no hematologic abnormalities were observed in FHZfp423-transduced mice, indicating that overexpression of *Zfp423* does not possess a transforming ability on primary hematopoietic cells, which is in accordance with the result that introduction of *Zfp423* in BM cells did not apparently increase colony numbers (Figure 3B). As expected from the results of previous studies, most of the *p210BCR/ABL*-transduced mice developed CML, except 2 cases that developed acute myeloid leukemia (AML) and B-cell ALL (B-ALL, Figure 4B bottom panel, left bar). In contrast, mice transduced with both types of viruses died in a shortened period and exhibited different phenotypes. The mean survival periods of mice reconstituted with p210BCR/ABL+FHZfp423 and those reconstituted with p210BCR/ABL alone were 29.5 and 48 days, respectively (Figure 4B top panel, thick and thin continuous lines), and the difference was statistically significant ($P < .01$). In addition, compared with mice reconstituted with p210BCR/ABL, those reconstituted with p210BCR/ABL+FHZfp423 exhibited an increased incidence of B-ALL (Figure 5B bottom panel, right bar), although the difference was not statistically significant ($P = .119$), probably due to the limited sample numbers. These results demonstrated that *Zfp423* possesses a cooperative oncogenecity with *p210BCR/ABL* in vivo, which accelerated disease onset and induced a more aggressive phenotype mainly of B-cell lineage. The representative results of pathologic analyses of mice that developed CML by p210BCR/ABL and that developed B-ALL by p210BCR/ABL plus FHZfp423 are shown in Figure 4C and the results of flow cytometry of the latter are shown in Figure 4D. The expression of *p210BCR/ABL* and *Zfp423* mRNAs in tumors developed in p210BCR/ABL plus FHZfp423-transduced mice was confirmed by RT-PCR (Figure S6).

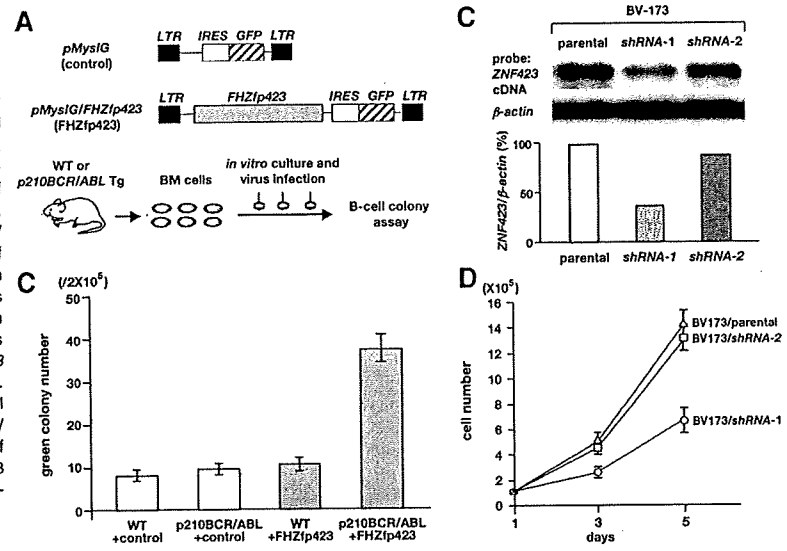

Figure 3. Effects of *Zfp423* expression on the colony formation and proliferation of *p210BCR/ABL*-expressing cells. (A) Schematic structures of the retroviruses and the illustration of the experimental procedure. BM cells were extracted from WT or *p210BCR/ABL* transgenic mice, infected with empty retrovirus (*pMyIG*, control) or *Flag-HA*–tagged *Zfp423 (FHZfp423)*–expressing retrovirus (*pMyIG*/FHZfp423, FHZfp423), and subjected to the B-cell colony assay. (B) Results of B-cell colony assay. The mean green colony number of 3 independent experiments for each group (WT+conrol, p210BCR/ABL+control, WT+FHZfp423, and p210BCR/ABL+FHZfp423) is shown with error bars. (C) Suppression of *ZNF423* expression by *shRNAs*. mRNA (5 μg) extracted from the parental BV-173 line and 2 *shRNA*-introduced sublines (*shRNA-1* and *shRNA*-2) were blotted with a part of the human *ZNF423* coding region. β-*Actin* hybridization was performed as an internal control and the relative expression ratio of *ZNF423* to β-*actin* in each cell line is shown as a vertical column. (D) Results of cell proliferation assay. Cells of the parental BV-173 line and 2 *shRNA*-introduced sublines (BV-173/*shRNA-1* and BV-173/*shRNA*-2) were plated at a density of 10^5/10 cm^2 on day 1 and cell numbers were counted on day 3 and day 5. The mean cell number of 3 independent experiments of each line is plotted with error bars.

Expression of *ZNF423* in human *BCR/ABL*-positive hematopoietic cell lines and CML BC samples

We finally investigated the clinical relevance of *ZNF423* expression in the progression from CML CP to BC using human Ph-positive hematopoietic cell lines and clinical samples. For the cell line experiment, cells expressing *p190BCR/ABL* (an alternative form of the *BCR/ABL* fusion gene) were also examined, because the expression of *p190BCR/ABL* is exclusively associated with B-ALL,[36] the same phenotype as the leukemias developed in the mice with *Zfp423* integration (nos. 18 and 23). In addition, Ph-negative B-ALL lines were included in this study to investigate the role of *ZNF423* in the development of B-cell malignancy without *BCR/ABL*.

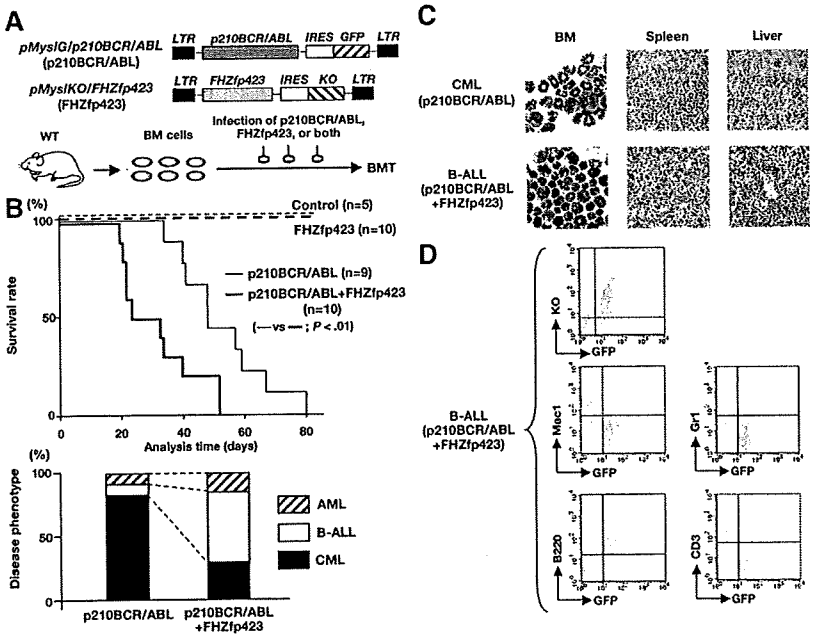

Figure 4. Survival and disease phenotype in mice that received a transplant of *p210BCR/ABL*- and/or *FHZfp423*-expressing BM cells. (A) Schematic structures of the retroviruses and the illustration of the experimental procedure. BM cells infected with *p210BCR/ABL*-expressing retrovirus (*pMyIG/p210BCR/ABL*), *FHZfp423*-expressing retrovirus (*pMyIKO/FHZfp423*), or both types of viruses were subjected to the BMT assay. KO indicates Kusabira Orange. (B) Acceleration of disease onset and altered disease phenotype by cotransduction of *Zfp423* and *p210BCR/ABL*. In the top panel, survival curves of mice reconstituted with BM cells transduced with control retrovirus (control, n = 5), *pMyIKO/FHZfp423* (FHZfp423, n = 10), *pMyIG/p210BCR/ABL* (p210BCR/ABL, n = 9), and both viruses (p210BCR/ABL+FHZfp423, n = 10) are shown as thin dotted, thick dotted, thin continuous, and thick continuous lines, respectively. In the bottom panel, the percentages of samples diagnosed as CML, B-ALL, and AML are shown by black, white, and shaded boxes, respectively. (C) Representative results of pathologic analysis of CML and B-ALL developed in mice transduced with p210BCR/ABL and p210BCR/ABL+FHZfp423, respectively. In the BM smears, proliferation of differentiated myeloid cells is observed in the CML case (top left panel), whereas monotonous proliferation of immature lymphoid tumor cells is apparent in the B-ALL case (bottom left panel). Massive infiltration of leukemic cells is shown in the spleen and liver (middle and right panels). (D) Representative results of flow cytometric analysis of B-ALL developed in mice transduced with p210BCR/ABL and FHZfp423. Leukemic cells are positive for both GFP and KO (top panel), confirming that they were originated from hematopoietic progenitor cells infected with both p210BCR/ABL and FHZfp423. GFP-positive leukemic cells showed positive staining for B220, but are negative for Mac-1, Gr-1, and CD3 (middle and bottom panels).

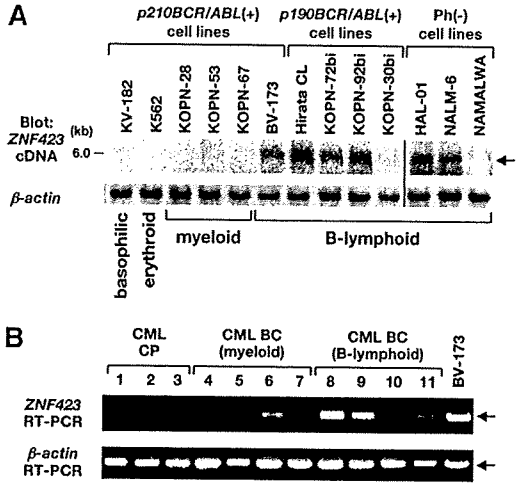

Figure 5. Expression of *ZNF423* in *BCR/ABL*-positive cell lines and in CML BC samples. (A) mRNA (3 μg) extracted from 6 *p210BCR/ABL*-positive, 4 *p190BCR/ABL*-positive, and 3 Ph-negative cell lines was blotted with a part of the human *ZNF423* coding region. β-*Actin* hybridization was performed as an internal control. The position of the *ZNF423* message is indicated by → and the immunophenotypes of the cell lines are shown at the bottom. A vertical line has been inserted to indicate a repositioned gel lane. (B) Total RNAs extracted BM samples from 3 CML CP and 8 CML BC cases (4 myeloid and 4 B-lymphoid) were subjected to RT-PCR for *ZNF423* expression. β-*Actin* RT-PCR was performed as an internal control.

mRNAs extracted from 6 *p210BCR/ABL*-positive cell lines (1 B-lymphoid, 3 myeloid, 1 erythroid, and 1 basophilic), 4 *p190BCR/ABL*-positive B-lymphoid cell lines, and 3 Ph-negative B-lymphoid cell lines were blotted with human *ZNF423* cDNA. As shown in Figure 5A, *ZNF423* mRNA expression was detected in 1 of 6 *p210BCR/ABL*-positive (BV-173), 3 of 4 *p190BCR/ABL*-positive (Hirata CL, KOPN-72bi, and KOPN-92bi), and 2 of 3 Ph-negative cell lines (HAL-01 and NALM-6), all of which were of B-cell phenotype.

We then examined *ZNF423* expression in human clinical samples diagnosed as CML CP or BC. BM samples of 3 CML CP and 4 CML BC patients (4 myeloid and 4 B-lymphoid lineages) with informed consent were subjected to RT-PCR using *ZNF423*-specific primers. BV-173 cells that express *ZNF423* (Figure 5A) were used as a control. As shown in Figure 5B, whereas no *ZNF423* expression was detected in CML CP sample (nos. 1-3), 4 of 8 CML BC samples were found to express *ZNF423*, where 1 was of myeloid (no. 6) and the other 3 were of B-lymphoid (nos. 8, 9, and 11) phenotypes. These results strongly indicated that aberrant expression of *ZNF423* clinically contributes to the malignant transformation of *BCR/ABL*-positive cells and to the progression to CML BC, mainly of B-cell lineage.

Discussion

CML provides an appropriate disease model for multistep carcinogenesis in which generation of p210BCR/ABL initiates CML CP and an additional genetic event(s) contributes to the evolution to CML BC.[8] We developed a transgenic mouse model for human CML, which expresses *p210BCR/ABL* in hematopoietic progenitor cells and reproducibly exhibits a CML-like myeloproliferative disorder.[14] To investigate molecular mechanism(s) responsible for disease progression, the *p210BCR/ABL* transgenic mice were subjected to retroviral insertional mutagenesis. BXH2 mice that harbor a horizontally transmittable replication-competent retrovirus[22] were used as a virus donor strain, because it has been successfully used to detect second hit genes in previous studies.[37-39]

The inbred BXH2 mice were reported to develop acute myeloid leukemia at 7 to 12 months of age due to ecotropic virus integration and intrinsic myeloid tropism.[22-24] In line with this report, all the WT/BXH2 mice died of myeloid leukemia (Figure 1A). In contrast, 6 p210BCR/ABL/BXH2 mice developed nonmyeloid leukemias with a shorter latency. The early disease onset and different phenotypes in these mice indicated that the diseases were caused by the cooperation of *p210BCR/ABL* with altered expression of virus-affected gene(s). Therefore, in this study, we intended to identify virus-integrated genes in the tumors of the 6 mice and iPCR analysis detected 2 CISs in B-cell leukemia samples. These CISs were considered to be strong candidates for CML BC, because leukemia with B-cell phenotype has not been detected in *p210BCR/ABL* transgenic mice[14] and very rarely reported in BXH2 mice (http://rtcgd.abcc.ncifcrf.gov/).[22,23,27]

It is to be noted that one CIS was in the promoter region of the transgene. Interestingly, our previous retrovirus insertional mutagenesis study, in which newborn *p210BCR/ABL* transgenic mice were directly injected with retroviruses, also identified the transgene as a CIS in B-cell BC cases, where retrovirus integration resulted in overexpression and/or enhanced kinase activity of the transgene product.[40] The up-regulation of *p210BCR/ABL* in the blast phase is especially interesting, because it corresponds to double Ph, which is one of the most frequently observed chromosomal abnormalities found in CML BC.[8] Therefore, our observation provides in vivo experimental evidence that acquired enhancement of *p210BCR/ABL* expression accelerates the disease and causes BC. The reason why mice with transgene integration exhibited B-cell leukemia is not clear. It could be possible that *p210BCR/ABL* originally expressed by the *TEC* promoter and then up-regulated by retrovirus insertion might predispose the infected mice to develop B-ALL by an unknown mechanism. In human CML BC, double Ph was reported to be occasionally associated with B-cell BC samples.[41,42]

Another CIS was the 5′ noncoding region of *Zfp423*, which encodes a transcription factor with multiple zinc-finger repeats.[33] Zfp423 was originally identified as a binding partner of Ebf (early B-cell factor, also denoted as Olf1), a protein essential for B-cell and olfactory nervous system development,[43,44] and was subsequently shown to interact with SMADs in response to bone morphogenic protein 2 (BMP2) in the *Xenopus laevis*.[45] *Zfp423* was also cloned as a target in B-cell lymphoma in AKXD27 mice by retroviral insertional mutagenesis.[33] In that study, retrovirus integration occurred upstream of the translation initiation codon resulting in a high level of expression, as observed in our cases (Figure 2).[33] A recent study demonstrated that *Zfp423* knockout mice exhibited abnormal cerebellum development but appeared to have a normal hematopoiesis,[46] suggesting that its ectopic expression would be involved in leukemogenesis.

It remains to be clarified how overexpression of *Zfp423* contributes to B-cell malignancy. Interestingly, although Zfp423 was originally identified as an Ebf-binding partner, it is not expressed in hematopoietic tissues including B cells.[33,34] In the olfactory nervous system, Zfp423 was shown to negatively regulate Ebf function; Zfp423 forms a heterodimer with Ebf, which inhibits Ebf homodimer formation that has an ability to transactivate downstream target genes.[43] Thus, it would be possible that the aberrant expression of *Zfp423* in the hematopoietic system induces B-cell leukemia, at least in part by impairing Ebf-mediated signaling. Alternatively, because a recent study demonstrated that a highly conserved 12–amino acid peptide located in the extreme

N-terminus of Zfp423 recruits the nucleosome remodeling and deacetylase corepressor complex (NuRD),[47] it could be postulated that Zfp423 functions as a transcription repressor and contributes to leukemogenesis by suppressing downstream target genes.

In this study, *Zfp423* was identified as a gene whose deregulated expression cooperates with *p210BCR/ABL* and induces CML BC. The cooperative activities of *Zfp423* and *p210BCR/ABL* were demonstrated by in vitro and in vivo mouse experiments and also by human samples. Enforced expression of *Zfp423* in hematopoietic cells derived from *p210BCR/ABL* transgenic mice enhanced B-cell colony formation, and suppression of *ZNF423* expression in *ZNF423*-expressing, *p210BCR/ABL*-positive CML BC cells reduced cell growth (Figure 3). In addition, expression of *Zfp423* with *p210BCR/ABL* in hematopoietic progenitor cells accelerated *p210BCR/ABL*-mediated leukemia and induced a more aggressive phenotype mainly of B-cell lineage (Figure 4). Furthermore, *ZNF423* is expressed in a subset of *BCR/ABL*-positive hematopoietic cell lines and several CML BC samples mostly with B-cell phenotype (Figure 5). These results demonstrated that *Zfp423/ZNF423* cooperates with *p210BCR/ABL*, confers a proliferative advantage to *p210BCR/ABL*-expressing hematopoietic cells, and consequently develops CML B-cell BC. It is to be noted that *ZNF423* expression was detected in several Ph-negative B-ALL lines (Figure 5), which indicates that *ZNF423* contributes not only to CML B-cell BC or Ph-positive B-ALL but also to de novo B-ALL without *BCR/ABL*.

It is intriguing that while the recipient mice transduced with both *p210BCR/ABL* and *Zfp423* developed mainly B-ALL, 2 cases developed AML (Figure 4B). Although *Zfp423* has been exclusively associated with B-ALL in retroviral insertional mutagenesis studies,[33,34] this result strongly suggests that *Zfp423* might contain a potency to develop AML as well as B-ALL. This idea is in accordance with the finding that one myeloid BC case expressed *ZNF423* in clinical analysis (Figure 5B no. 6). Recently, *Zfp521/ZNF521* (also known as *EHZF [early hematopoietic zinc finger protein]* and *Evi3*), which is homologous to *Zfp423/ZNF423* and was also identified as a target of B-ALLs by mouse retrovirus insertional mutagenesis studies,[34,48] was reported to be frequently involved in AML samples in human leukemias.[49] Thus, a set of zinc finger–containing transcription factors that has been isolated as a target in B-ALL in mice might contribute to leukemias with different phenotypes in humans.

As for the 2 mice that developed T-ALL, although we could not identify any CIS, candidate genes, such as *Hcst (hematopoietic cell signal transducer,* also called *DAP10/KAP10*), an adaptor protein involved in T-cell signaling,[50,51] and *Il21r* (*IL21 receptor*), a cytokine receptor mediating T-cell activation[52,53] were detected (Table S1). In addition, several genes isolated by iPCR have been reported in cancer gene studies. For example, *Avpil1, Ddx6, Runx1, Mef2d, Jak1, Cbfa2t3h,* and *Sox4* have already been identified as retrovirus integration sites in the mouse retrovirus tagged cancer gene database (RTCGD; http://rtcgd.abcc.ncifcrf.gov/),[23,27] and *IL21R, DDx6, Runx1,* and *Cbfa2t3h* have been denoted as chromosomal translocation-associated genes in human cancer (http://www.sanger.ac.uk/genetics/CGP/Census/).[54] Furthermore, *MEF2D* was shown to create a fusion gene in t(1;19)(q23;p13),[55] and *Sox4* was demonstrated to be a powerful tool to identify cooperative genes when transplanted by a replication-defective retrovirus.[56] Further studies will be required to investigate whether virus insertion in these genes might affect the BC phenotype and/or lineage commitment observed in p210BCR/ABL/BXH2 mice.

In this study, we demonstrated that enhanced expression of *p210BCR/ABL* and aberrant expression of *Zfp423/ZNF423* contribute to blastic transformation of *p210BCR/ABL*-expressing hematopoietic cells. Our results provide insights into the molecular mechanism(s) for disease progression of human CML and prove this transgenic system is a valuable tool in identifying genes whose altered expression cooperates with *p210BCR/ABL* to induce CML BC.

Acknowledgments

We thank Yuki Sakai, Kayoko Hashimoto, and Yuko Tsukawaki for the mouse care and technical assistance; Tomoko Takahara and Yukari Yamazaki for BMT studies; and Hirotaka Matsui for the statistical analysis. We also thank Motomi Osato for helpful discussion and Hiroya Aso and Toshiya Inaba for providing us with Ph-positive human hematopoietic cell lines.

This work was supported by a Grant-in-Aid from the Ministry of Education, Science and Culture of Japan (Tokyo, Japan), a Grant-in-Aid for Cancer Research from the Ministry of Health, Labor and Welfare of Japan (13-2; Tokyo, Japan) Research Grant of the Princess Takamatsu Cancer Research Fund (Tokyo, Japan), Mitsubishi Pharma Research Foundation (Osaka, Japan), YASUDA Medical Research Foundation (Osaka, Japan), a Grant-in-Aid of The Japan Medical Association (Tokyo, Japan), and Japan Leukemia Research Fund (Tokyo, Japan).

Authorship

Contribution: K.M., N.Y., M.M., T.N., and H.H. designed and performed the research and wrote the paper; H.O. centralized the pathologic analysis; Y. Komeno, J.K., Z.-i.H., and T. Kitamura, performed the retrovirus and shRNA studies; S.W., N.A.J., and N.G.C. participated in the Zfp423 studies and wrote the paper; T. Kuwata, Y. Kanno, and T.N. contributed to the BMT analysis; and all the authors checked and agreed on the final version of the paper.

Conflict-of-interest disclosure: The authors declare no competing financial interests.

Correspondence: Hiroaki Honda, Department of Developmental Biology, Research Institute of Radiation Biology and Medicine, Hiroshima University, 1-2-3 Kasumi, Minami-ku, Hiroshima 734-8553, Japan; e-mail: hhonda@hiroshima-u.ac.jp.

References

1. Deininger MWN, Goldman JM, Melo JV. The molecular biology of chronic myeloid leukemia. Blood. 2000;96:3343-3356.
2. Ren R. Mechanisms of BCR-ABL in the pathogenesis of chronic myelogenous leukaemia. Nat Rev Cancer. 2005;5:172-183.
3. Rowley JD. A new consistent chromosomal abnormality in chronic myelogenous leukemia identified by quinacrine fluorescence and Giemsa staining. Nature. 1973;243:290-293.
4. de Klein A, van Kessel AG, Grosveld G, et al. A cellular oncogene is translocated to the Philadelphia chromosome in chronic myelocytic leukaemia. Nature. 1982;300:765-767.
5. Groffen J, Stephenson JR, Heisterkamp N, deKlein A, Bartram CR, Grosveld G. Philadelphia chromosomal breakpoints are clustered within a limited region, bcr, on chromosome 22. Cell. 1984;36:93-99.
6. Shtivelman E, Lifshitz B, Gale RP, Canaani E. Fused transcript of abl and bcr genes in chronic myelogenous leukaemia. Nature. 1985;315:550-554.
7. Konopka JB, Watanabe SM, Witte ON. An alternation of the human c-abl protein in K562 leukemia cells unmasks associated tyrosine kinase activity. Cell. 1984;37:1035-1042.

8. Calabretta B, Perrotti D. The biology of CML blast crisis. Blood. 2004;103:4010-4022.
9. Pear WS, Miller JP, Xu L, et al. Efficient and rapid induction of a chronic myelogenous leukemia-like myeloproliferative disease in mice receiving P210 bcr/abl-transduced bone marrow. Blood. 1998;92: 3780-3792.
10. Zhang X, Ren R. Bcr-Abl efficiently induces a myeloproliferative disease and production of excess interleukin-3 and granulocyte-macrophage colony-stimulating factor in mice: a novel model for chronic myelogenous leukemia. Blood. 1998;92:3829-3840.
11. Li S, Ilaria RLJ, Million RP, Daley GQ, Van Etten RA. The P190, P210, and P230 forms of the BCR/ABL oncogene induce a similar chronic myeloid leukemia-like syndrome in mice but have different lymphoid leukemogenic activity. J Exp Med. 1999;189:1399-1342.
12. Honda H, Fujii T, Takatoku M, et al. Expression of p210bcr/abl by metallothionein promoter induced T-cell leukemia in transgenic mice. Blood. 1995; 85:2853-2861.
13. Voncken JW, Kaartinen V, Pattengale PK, Germeraad WTV, Groffen J, Heisterkamp N. BCR/ABL p210 and p190 cause distinct leukemia in transgenic mice. Blood. 1995;86:4603-4611.
14. Honda H, Oda H, Suzuki T, et al. Development of acute lymphoblastic leukemia and myeloproliferative disorder in transgenic mice expressing p210bcr/abl: a novel transgenic model for human Ph1-positive leukemias. Blood. 1998;91:2067-2075.
15. Huettner CS, Zhang P, Van Etten RA, Tenen DG. Reversibility of acute B-cell leukaemia induced by BCR-ABL1. Nat Genet. 2000;24:57-60.
16. Huettner CS, Koschmieder S, Iwasaki H, et al. Inducible expression of BCR/ABL using human CD34 regulatory elements results in a megakaryocytic myeloproliferative syndrome. Blood. 2003;102:3363-3370.
17. Koschmieder S, Gottgens B, Zhang P, et al. Inducible chronic phase of myeloid leukemia with expansion of hematopoietic stem cells in a transgenic model of BCR-ABL leukemogenesis. Blood. 2005;105:324-334.
18. Honda H, Yamashita Y, Ozawa K, HM. Cloning and characterization of mouse tec promoter. Biochem Biophys Res Commun. 1996;223:422-426.
19. Honda H, Ozawa K, Yazaki Y, Hirai H. Identification of PU. 1 and Sp1 as essential transcriptional factors for the promoter activity of mouse tec gene. Biochem Biophys Res Comm. 1997;234: 376-381.
20. Honda H, Ushijima T, Wakazono K, et al. Acquired loss of p53 induces blastic transformation in p210bcr/abl-expressing hematopoietic cells: a transgenic study for blast crisis of human CML. Blood. 2000;95:1144-1150.
21. Niki M, Cristofano DA, Zhao M, et al. Role of Dok-1 and Dok-2 in leukemia suppression. J Exp Med. 2004;200:1689-1695.
22. Li J, Shen H, Himmel KL, et al. Leukaemia disease genes: large-scale cloning and pathway predictions. Nat Genet. 1999;23:348-353.
23. Akagi K, Suzuki T, Stephens RM, Jenkins NA, Copeland NG. RTCGD: retroviral tagged cancer gene database. Nucleic Acids Res. 2004;32(database issue):D523-D527.
24. Turcotte K, Gauthier S, Tuite A, Mullick A, Malo D, Gros P. A mutation in the Icsbp1 gene causes susceptibility to infection and a chronic myeloid leukemia-like syndrome in BXH-2 mice. J Exp Med. 2005;201:881-890.
25. Miyazaki K, Kawamoto T, Tanimoto K, Nishiyama M, Honda H, Kato Y. Identification of functional hypoxia response elements in the promoter region of the DEC1 and DEC2 genes. J Biol Chem. 2002;277:47014-47021.
26. University of Colombo School of Computing. UCSC Genome Browser. http://genome.ucsc.edu. Accessed January 2009.
27. National Cancer Institute–Frederick. Mouse Retrovirus Tagged Cancer Gene Database. http://rtcgd.abcc.ncifcrf.gov. Accessed January 2009.
28. Kitamura T, Koshino Y, Shibata F, et al. Retrovirus-mediated gene transfer and expression cloning: powerful tools in functional genomics. Exp Hematol. 2003;31:1007-1014.
29. Morita S, Kojima T, Kitamura T. Plat-E: an efficient and stable system for transient packaging of retroviruses. Gene Ther. 2000;7:1063-1066.
30. Jin G, Yamazaki Y, Takuwa M, et al. Trib1 and Evi1 cooperate with Hoxa and Meis1 in myeloid leukemogenesis. Blood. 2007;109:3998-4005.
31. Kono H, Kyogoku C, Suzuki T, et al. FcgammaRIIB Ile232Thr transmembrane polymorphism associated with human systemic lupus erythematosus decreases affinity to lipid rafts and attenuates inhibitory effects on B cell receptor signaling. Hum Mol Genet. 2005;14:2881-2892.
32. Harada H, Harada Y, Tanaka H, Kimura A, Inaba T. Implications of somatic mutations in the AML1 gene in radiation-associated and therapy-related myelodysplastic syndrome/acute myeloid leukemia. Blood. 2003;101:673-680.
33. Warming S, Suzuki T, Yamaguchi TP, Jenkins NA, Copeland NG. Early B-cell factor-associated zinc-finger gene is a frequent target of retroviral integration in murine B-cell lymphomas. Oncogene. 2004;23:2727-2731.
34. Warming S, Liu P, Suzuki T, et al. Evi3, a common retroviral integration site in murine B-cell lymphoma, encodes an EBFAZ-related Kruppel-like zinc finger protein. Blood. 2003;101:1934-1940.
35. Sanuki S, Hamanaka S, Kaneko S, et al. A new red fluorescent protein that allows efficient marking of murine hematopoietic stem cells. J Gene Med. 2008;10:965-971.
36. Pane F, Intrieri M, Quintarelli C, Izzo B, Muccioli GC, Salvatore F. BCR/ABL genes and leukemic phenotype: from molecular mechanisms to clinical correlations. Oncogene. 2002;21:8652-8667.
37. Iwasaki M, Kuwata T, Yamazaki Y, et al. Identification of cooperative genes for NUP98-HOXA9 in myeloid leukemogenesis using a mouse model. Blood. 2005;105:784-793.
38. Yanagida M, Osato M, Yamashita N, et al. Increased dosage of Runx1/AML1 acts as a positive modulator of myeloid leukemogenesis in BXH2 mice. Oncogene. 2005;24:4477-4485.
39. Yamashita N, Osato M, Huang L, et al. Haploinsufficiency of Runx1/AML1 promotes myeloid features and leukaemogenesis in BXH2 mice. Br J Haematol. 2005;131:495-507.
40. Mizuno T, Yamasaki N, Miyazaki K, et al. Overexpression/enhanced kinase activity of BCR/ABL and altered expression of Notch1 induced acute leukemia in p210BCR/ABL transgenic mice. Oncogene. 2008;27:3465-3474.
41. Tien HF, Chuang SM, Wang CH, et al. Chromosomal characteristics of Ph-positive chronic myelogenous leukemia in transformation: a study of 23 Chinese patients in Taiwan. Cancer Genet Cytogenet. 1989;39:89-97.
42. Griesshammer M, Heinze B, Bangerter M, Heimpel H, Fliedner TM. Karyotype abnormalities and their clinical significance in blast crisis of chronic myeloid leukemia. J Mol Med. 1997;75: 836-838.
43. Tsai RY, Reed RR. Cloning and functional characterization of Roaz, a zinc finger protein that interacts with O/E-1 to regulate gene expression: implications for olfactory neuronal development. J Neurosci. 1997;17:4159-4169.
44. Tsai RY, Reed RR. Identification of DNA recognition sequences and protein interaction domains of the multiple-Zn-finger protein Roaz. Mol Cell Biol. 1998;18:6447-6456.
45. Hata A, Seoane J, Lagna G, Montalvo E, Hemmati-Brivanlou A, Massague J. OAZ uses distinct DNA- and protein-binding zinc fingers in separate BMP-Smad and Olf signaling pathways. Cell. 2000;100:229-240.
46. Warming S, Rachel RA, Jenkins NA, Copeland NG. Zfp423 is required for normal cerebellar development. Mol Cell Biol. 2006;26: 6913-6922.
47. Lauberth SM, Rauchman MA. Conserved 12-amino acid motif in Sall1 recruits the nucleosome remodeling and deacetylase corepressor complex. J Biol Chem. 2006;281:23922-23931.
48. Hentges KE, Weiser KC, Schountz T, Woodward LS, Morse HC, Justice MJ. Evi3, a zinc-finger protein related to EBFAZ, regulates EBF activity in B-cell leukemia. Oncogene. 2005; 24:1220-1230.
49. Bond HM, Mesuraca M, Amodio N, et al. Early hematopoietic zinc finger protein-zinc finger protein 521: a candidate regulator of diverse immature cells. Int J Biochem Cell Biol. 2008;40:848-854.
50. Wu J, Song Y, Bakker AB, et al. An activating immunoreceptor complex formed by NKG2D and DAP10. Science. 1999;285:730-732.
51. Chang C, Dietrich J, Harpur AG, et al. Cutting edge: KAP10, a novel transmembrane adapter protein genetically linked to DAP12 but with unique signaling properties. J Immunol. 1999; 163:4651-4654.
52. Mehta DS, Wurster AL, Grusby MJ. Biology of IL-21 and the IL-21 receptor. Immunol Rev. 2004; 202:84-95.
53. Leonard WJ, Spolski R. Interleukin-21: a modulator of lymphoid proliferation, apoptosis and differentiation. Nat Rev Immunol. 2005;5:688-698.
54. Wellcome Trust Sanger. Cancer Gene Census. http://www.sanger.ac.uk/genetics/CGP/Census. Accessed _.
55. Yuki Y, Imoto I, Imaizumi M, et al. Identification of a novel fusion gene in a pre-B acute lymphoblastic leukemia with t(1;19)(q23;p13). Cancer Sci. 2004;95:503-507.
56. Du Y, Spence SE, Jenkins NA, Copeland NG. Cooperating cancer-gene identification through oncogenic-retrovirus-induced insertional mutagenesis. Blood. 2005;106:2498-2505.

Research Article

p53-Altered *FBXW7* Expression Determines Poor Prognosis in Gastric Cancer Cases

Takehiko Yokobori,[1,2] Koshi Mimori,[1] Masaaki Iwatsuki,[1] Hideshi Ishii,[1] Ichiro Onoyama,[3] Takeo Fukagawa,[4] Hiroyuki Kuwano,[2] Keiichi I. Nakayama,[3] and Masaki Mori[5]

[1]Department of Surgery, Medical Institute of Bioregulation, Kyushu University, Beppu, Japan; [2]Departments of General Surgical Science, Graduate School of Medicine, Gunma University, Maebashi, Japan; [3]Department of Molecular and Cellular Biology, Medical Institute of Bioregulation, Kyushu University, Fukuoka, Japan; [4]Department of Surgery, National Cancer Center Hospital, Tokyo, Japan; and [5]Department of Gastroenterological Surgery, Graduate School of Medicine, Osaka University, Suita, Japan

Abstract

A molecular target associated with the progression of gastric cancer has not yet been uncovered. *FBXW7* is a tumor suppressor gene transcriptionally controlled by p53 that plays a role in the regulation of cell cycle exit and reentry via c-Myc degradation. Few studies have addressed the clinical significance of *FBXW7* expression in gastric cancer. Therefore, we examined *FBXW7* mRNA expression to determine its clinicopathologic significance in 100 cases of gastric cancer. Low expression levels of *FBXW7* in primary gastric cancer contributed to malignant potential, such as lymph node metastasis ($P = 0.0012$), tumor size ($P = 0.0003$), and poor prognosis ($P = 0.018$). In comparison with 52 cases of gastric cancer without the *p53* mutation, 29 cases with the mutation exhibited lower expression levels of *FBXW7* ($P = 0.0034$), revealing a significant relationship between *p53* mutation and *FBXW7* expression. Furthermore, we found that gastric cancer patients who had low *FBXW7* expression levels and *p53* mutation had a distinctively poor prognosis in comparison with other subgroups ($P = 0.0033$). In conclusion, we showed a role for *p53* in the transcriptional regulation of *FBXW7* expression in clinical gastric cancer cases and showed that disruption of both *p53* and *FBXW7* contributes to poor prognosis. [Cancer Res 2009;69(9):3788–94]

Introduction

FBXW7 is a F-box protein subunit of a SCF-type ubiquitin ligase complex that induces the degradation of positive cell cycle regulators (oncoproteins) such as c-Myc, cyclin E, c-Jun, and Notch. Therefore, *FBXW7* and the associated molecules have been focused on as one of the new carcinoma control structures (1, 2). In particular, *FBXW7* induces cell cycle exit (G_0 phase) via c-Myc degradation, so the altered expression of *FBXW7* is considered one of the major causes of carcinogenesis or carcinoma development (2–4). Because *FBXW7* also participates in cell cycle exit to, and the reentry from, G_0 (5–7), it is a candidate molecular therapeutic target in intractable carcinoma cases that are firmly resistant to combined modality therapies (5, 8).

Mao and colleagues reported that epithelial tumors are not established in $p53^{-/-}$ mice, whereas $p53^{+/-}$ mice form epithelial tumors with altered *FBXW7* expression. *FBXW7* works downstream of *p53*, both of these cell cycle regulator genes, are critical for carcinogenesis of epithelial tissues (3).

Recently, Onoyama and colleagues reported that mice carrying a *FBXW7* T-cell conditional knockout eventually developed thymic lymphomas following thymomas. *FBXW7* and *p53* double-knockout mice developed thymic lymphomas more frequently than other subgroups of knockout mice, such as wild-type, $p53^{-/-}$, and *FBXW7* conditional knockout mice. Therefore, their study clearly showed the consecutive roles of p53 and FBXW7 in the carcinogenesis of solid tumors *in vivo*. Moreover, a comparison of four groups classified according to *FBXW7* and *p53* status revealed a worse prognosis for double inactivation mice than in the other subgroups (6). It is unknown if identical findings were observed during previous *in vivo* studies of human cancer cases.

The clinical significance of *FBXW7* in human solid cancers has been diversely reported. *FBXW7* mutation rates in cholangiocarcinomas, T-cell acute lymphocytic leukemia, endometrial carcinoma, and colorectal cancer were reported as 35%, 31%, 9%, and 9%, respectively (2, 4, 9, 10). Also, *FBXW7* low expression in glioma tissues reportedly produces a poor prognosis (11, 12). Lee and colleagues reported that the *FBXW7* mutation rate in clinical gastric cancer tissues of 3.7% to 6% did not differ in early or progressive gastric cancer (4, 13). However, few studies are available on the connection between *FBXW7* expression level and poor prognoses in gastric cancer.

This study details (*a*) the magnitude of the effect of altered *FBXW7* expression on prognosis determination in gastric cancer cases; (*b*) the significance of both *FBXW7* expression and *p53* mutation status on clinical gastric cancer cases, which was compared with previous *in vivo* reports; and (*c*) how the coexistence of the *p53* mutation and low expression of *FBXW7* in clinical samples determines malignant potential and a poorer prognosis for gastric cancer patients.

Materials and Methods

Clinical samples and cell lines. One hundred gastric cancer samples and paired noncancerous samples were obtained during surgery and used after obtaining informed consent. All patients underwent resection of the primary tumor at Kyushu University Hospital at Beppu and affiliated hospitals between 1992 and 2000. Resected cancer tissues and paired noncancerous tissues were immediately cut and embedded in Tissue-Tek OCT medium (Sakura), frozen in liquid nitrogen, and kept at −80°C until RNA and DNA extraction. Following isolation of RNA and DNA, cDNA was synthesized from 8.0 μg total RNA as described previously (14).

The human gastric cancer cell line AZ521 was provided by the Cell Resource Center of Biomedical Research, Institute of Development, Aging

Note: Supplementary data for this article are available at Cancer Research Online (http://cancerres.aacrjournals.org/).

Requests for reprints: Masaki Mori, Department of Gastroenterological Surgery, Graduate School of Medicine, Osaka University, 2-2 Yamadaoka, Suita 565-0871, Japan. Phone: 81-6-6879-3251; Fax: 81-6-6879-3259; E-mail: mmori@gesurg.med.osaka-u.ac.jp.

doi:10.1158/0008-5472.CAN-08-2846

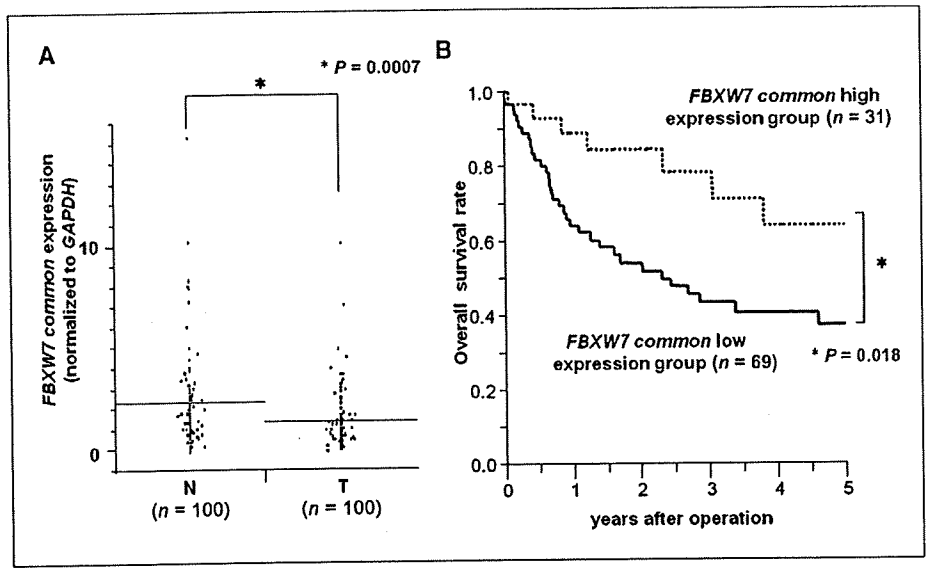

Figure 1. Clinical significance of *FBWX7* mRNA expression in clinical samples. *A*, *FBXW7* mRNA expression in cancer (*T*) and noncancerous (*N*) tissues from gastric cancer patients by real-time reverse transcription-PCR (n = 100). *FBXW7* (T; n = 100), *FBXW7* mRNA (T)/*GAPDH* mRNA (T); *FBXW7* (N; n = 100), *FBXW7* mRNA (N)/*GAPDH* mRNA (N). *Horizontal lines*, mean. *B*, Kaplan-Meier overall survival curves of gastric cancer patients according to the level of *FBXW7* mRNA expression. The high *FBXW7* expression group (n = 31), *FBXW7* (T)/*FBXW7* (N) ≥ 1.0; low *FBXW7* expression group (n = 69), *FBXW7* (T)/*FBXW7* (N) < 1.0.

and Cancer, Tohoku University. This cell line was maintained in RPMI 1640 containing 10% fetal bovine serum with 100 units/mL penicillin and 100 units/mL streptomycin sulfates and cultured in a humidified 5% CO_2 incubator at 37°C.

Real-time quantitative reverse transcription-PCR. *FBXW7*-specific oligonucleotide primers were designed to amplify a 249-bp PCR product encoding the common region among three *FBXW7* isoforms. The following primers were used: *FBXW7* sense primer 5′-AAAGAGTTGTTAGCGGTTCTCG-3′ and antisense primer 5′-CCACATGGATACCATCAAACTG-3′ and glyceraldehyde-3-phosphate dehydrogenase (*GAPDH*; 270 bp) sense primer 5′-GTCAACGGATTTGGTCTGTATT-3′ and antisense primer 5′-AGTCTTCTGGGTGGCAGTGAT-3′. These primers spanned more than two exons to avoid amplification of contaminating genomic DNA. PCR amplification for quantification of *FBXW7* and *GAPDH* mRNA in clinical samples was done in the LightCycler system (Roche Applied Science) using the LightCycler-FastStart DNA Master SYBR Green I Kit (Roche Applied Science) as described previously (15). The amplification conditions of cycles consisted of initial denaturation at 95°C for 10 min followed by 40 cycles of denaturation at 95°C for 10 s, annealing at 62°C (60°C for *GAPDH*) for 10 s, and elongation at 67°C (65°C for *GAPDH*) for 10 s. Melting curve analysis was done to distinguish specific products from nonspecific products and primer dimmers. The relative expression levels of *FBXW7* were obtained by normalizing the amount of *FBXW7* mRNA divided by that of *GAPDH* mRNA as an endogenous control in each sample.

FBXW7 RNA interference. *FBXW7*-specific siRNA (Silencer Predesigned siRNA1: sense GCACAGAAUUGAUACUAACTT and antisense GUUAGUAUCAAUUCUGUGCTG and Silencer Predesigned siRNA2: sense CCUUAUAUGGGCAUACUUCTT and antisense GAAGUAUGCCCAUAUAAGGTG) and negative control siRNA (Silencer Negative Control 1 siRNA) were purchased from Ambion. Lipofectamine RNA interference MAX (Invitrogen) and *FBXW7*-specific siRNA were then added in 6-well flat-bottomed microtiter plates. After incubation, the AZ521 cell line was seeded at 1.5 × 10^5 per well in a volume of 2 mL in 6-well flat-bottomed microtiter plates and incubated in a humidified atmosphere (37°C and 5% CO_2). The RNA interference assay was done after a 24 h incubation.

Immunoblot analysis. Total protein was extracted from AZ521 after *FBXW7* RNA interference. Aliquots of total protein (35 μg) were electrophoresed in 7.5% concentrated READY GELS J (Bio-Rad Laboratories). c-Myc, cyclin E, and p53 proteins were detected using anti-c-Myc (N-262), anti-cyclin E (M-20), and anti-p53 (Pab240; all obtained from Santa Cruz Biotechnology) diluted 1:500, 1:100, and 1:100, respectively. These proteins were normalized to the level of β-actin protein (Cytoskeleton) diluted 1:1,000. Western blot analysis was done as described previously (16). Enhanced chemiluminescence detection reagents (Amersham Biosciences) were used to detect antigen-antibody reactions.

***In vitro* proliferation assay.** Proliferation was determined using the 3-(4,5-dimethylthiazol-2-yl)-2,5-diphenyltetrazolium bromide assay (Roche Diagnostics). After a 24 h incubation following siRNA addition, cells were cultured further for 0 to 72 h and the absorbance of the samples was measured as described previously (17).

***p53* and *FBXW7* sequence.** Among 100 gastric cancer samples in which *FBXW7* mRNA levels were measured, *p53* was sequenced in 81 genomic DNA samples. Similarly, 80 paired cDNA samples were subjected to *FBXW7* mutational analysis.

The 81 genomic DNA samples were used as templates to PCR amplify exons 4 to 9 of the *p53* gene with primers derived from intronic sequences (Supplementary Table S1). The PCR was done with AmpliTaq Gold DNA Polymerase (Applied Biosystems). Likewise, the *FBXW7* (α, β, and γ) sequence was amplified using cDNA from 80 gastric cancer samples with KOD-FX DNA polymerase (TOYOBO) and sequencing primers (Supplementary Table S1). These PCR products were electrophoresed on 1% agarose gels containing ethidium bromide and purified with ethanol precipitation. Purified PCR products were sequenced using a Big-Dye Terminator version 1.1 Cycle Sequencing Kit (Applied Biosystems) and an ABI3100 sequencer (Applied Biosystems).

Statistical analysis. Differences between two groups were estimated with Student's t test, χ^2 analysis, and ANOVA. Overall survival curves were plotted according to the Kaplan-Meier method, with the log-rank test applied for comparison. Survival was measured from the day of the surgery. Data for *FBXW7* mRNA expression levels in three groups were analyzed with ANOVA. When the results of the ANOVA were significant, Tukey's multiple comparison tests were used to assess differences in *FBXW7* mRNA expression levels among each group. All differences were statistically significant at the level of $P < 0.05$ and a tendency was indicated at the level of $P < 0.1$. Statistical analyses were done using the JMP 5 for Windows software package (SAS Institute).

Results

Clinical significance of *FBXW7* mRNA expression in gastric cancer cases. The expression levels of *FBXW7* mRNA in cancerous tissues (n = 100) and paired noncancerous tissues (n = 100) of the gastric cancer patients were examined by real-time reverse transcription-PCR. These data were corrected for *GAPDH* mRNA levels. *FBXW7* mRNA expression levels in cancer

tissues (mean ± SD, 1.41 ± 1.51) were lower than those in noncancerous tissues (2.37 ± 2.3). A significant difference in mRNA mean expression level was found between cancerous and noncancerous tissues (P = 0.0007; Fig. 1*A*). Immunostaining of FBXW7 was done to confirm the correlation between *FBXW7* mRNA and FBXW7 protein. Fifteen gastric cancer samples were divided into two groups according to FBXW7 protein level (high or low). The expression of *FBXW7* mRNA in each group was examined and compared with protein expression levels. The high FBXW7 protein group (n = 7) showed high *FBXW7* mRNA expression levels in comparison with the low FBXW7 protein group (n = 8; P = 0.0013; Supplementary Fig. S1).

In the overall survival curve (Fig. 1*B*), patients in the low *FBXW7* expression group (n = 69; cancer/noncancerous tissues < 1.0) had a significantly poorer prognosis than those in the high *FBXW7* expression group (n = 31; cancer/noncancerous tissues ≥ 1.0; P = 0.018). However, there was no relationship between *FBXW7* expression and clinical stage progression (Supplementary Fig. S2). Multivariate analysis revealed that the *FBXW7* mRNA expression level in cancer is an independent predictor of lymph node metastasis (Supplementary Table S2*A* and B).

Table 1. *FBXW7* gene expression and clinicopathologic factors for 100 gastric cancer patients

	FBXW7/GAPDH		*P*
	High expression (n = 31)	Low expression (n = 69)	
Age (y)			
≥65	15	30	0.69
<65	16	38	
Gender			
Male	17	49	0.12
Female	14	20	
Histology			
Well, moderate	16	34	0.88
Poor, signet	15	34	
Size (cm)			
<5	22	22	0.0003*
≥5	9	47	
Depth			
T_1 (m, sm)	10	11	0.06†
T_2-T_4 (mp, ss, se, si)	21	58	
Lymph node metastasis			
Absent	18	17	0.0012*
Present	13	52	
Lymphatic invasion			
Absent	12	17	0.15
Present	19	52	
Venous invasion			
Absent	27	45	0.024*
Present	4	24	
Liver metastasis			
Absent	31	65	0.17
Present	0	4	
Peritoneal dissemination			
Absent	30	53	0.014*
Present	1	16	
Stage			
I, II	23	28	0.0019*
III, IV	8	41	

NOTE: High *FBXW7* expression group (n = 31), *FBXW7* (T)/*FBXW7* (N) < 1.0; low *FBXW7* expression group (n = 69), *FBXW7* (T)/*FBXW7* (N) < 1.0. Well, well differentiated; poor, poorly differentiated; moderate, moderately differentiated; signet, signet ring cell.
*P < 0.05.
†P < 0.1.

Clinicopathologic factors were significantly different in the low *FBXW7* expression group (n = 69). There was more progressive tumor size, lymph node metastasis, venous invasion, peritoneal dissemination, and clinical staging compared with the high *FBXW7* expression group (n = 31; P < 0.05). However, no significant differences were observed regarding age, gender, histology, lymphatic invasion, and liver metastasis (Table 1).

Expression of the *FBXW7* isoform and prognosis in gastric cancer cases. In several *in vivo* studies, mouse *Fbxw7* has three isoforms (α, β, and γ). The α isoform is expressed in most tissues, the β isoform is found in the brain and testis, and the γ isoform is in the heart and muscle (5). We confirmed the distribution of *FBXW7* expression in a human panel before searching for *FBXW7* mutations in gastric cancer cases. We found a similar distribution of *FBXW7* mRNA expression between the human panel and laboratory mice (Supplementary Fig. S3). *Fbxw7* γ controls the nucleolar level of c-Myc and cell size and is restricted to muscle cells, which is larger than other cells (5, 18). It has been suggested that *Fbxw7* γ contributes to muscle differentiation through regulation of c-Myc. Therefore, the expression level of *FBXW7* γ in the heart might be very high to regulate heart muscle differentiation (Supplementary Fig. S3).

In addition, the association between overall *FBXW7* expression and poor prognosis was more significant than between the expression of any individual isoform (Supplementary Fig. S4).

***FBXW7* and *p53* mutation analysis.** We examined *p53* mutations in 81 genomic DNA samples and *FBXW7* mutations in 80 cDNA samples, the same paired samples that were used for the *FBXW7* mRNA expression assay. Mutation analysis done with sequencing found *p53* and *FBXW7* mutation rates of 35.8% (29 of 81) and 8.8% (7 of 80), respectively (Fig. 2*A* and *B*; Supplementary Table S3; Supplementary Fig. S5).

Examination of the relationship between *p53* mutation status and *FBXW7* mRNA expression levels revealed that *FBXW7* mRNA mean expression levels in the *p53* mutation (+) group (n = 29; 1.07 ± 1.03) were lower than those in the *p53* mutation (−; n = 52; 1.56 ± 1.79) and noncancerous tissues (n = 100; 2.36 ± 2.3). A significant difference was found between the *p53* mutation (+) group and the other groups (Fig. 3). In addition, no difference was observed between the *p53* mutation (−) gastric cancer tissues and noncancerous tissues.

Mean expression levels of *FBXW7* in the *FBXW7* mutation (+) group (n = 7) were not significantly different from those of the *FBXW7* mutation (−) group (n = 73) and noncancerous tissues (n = 100). The presence of the *FBXW7* mutation was not associated with poor prognosis or clinical stage in gastric cancer patients (Supplementary Fig. S5).

***FBXW7* RNA interference promotes proliferation *in vitro*.** Because *FBXW7* mRNA suppression in cancer tissues is associated with poor prognosis, the protein levels of c-Myc and cyclin E, degradation targets of *FBXW7*, were examined to evaluate *FBXW7* function in gastric cancer cells. *FBXW7*

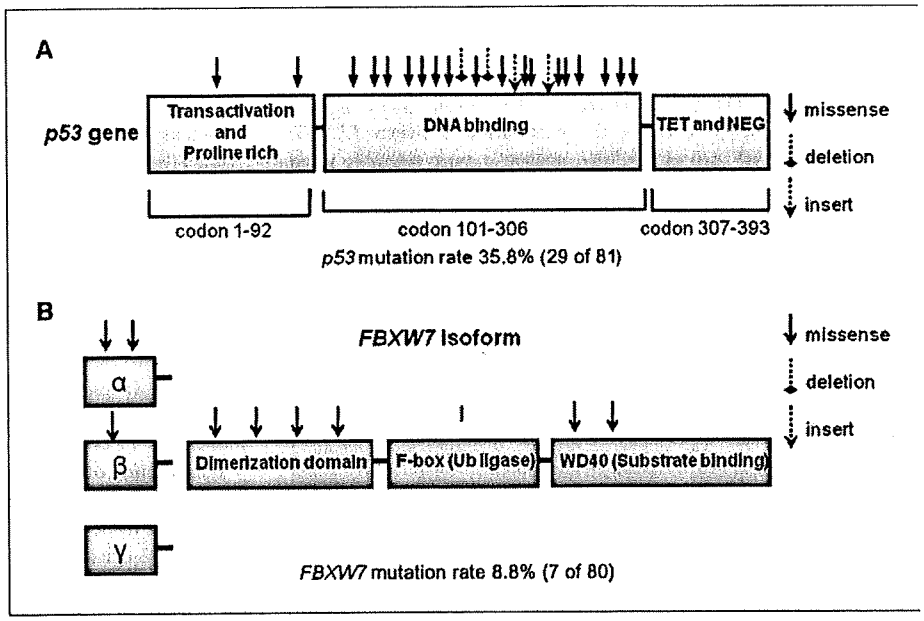

Figure 2. *p53* and *FBXW7* mutation analysis. *A*, structure and mutation of the *p53* gene in gastric cancer patients (n = 81). *B*, structure and mutation of the *FBXW7* gene in gastric cancer patients (n = 80). *Arrows*, mutation type, such as missense, deletion, and insertion.

suppression analysis was done with two different *FBXW7* siRNA (siRNA1 or siRNA2) using gastric cancer cell line AZ521. *FBXW7* suppression by siRNA was confirmed with quantitative reverse transcription-PCR in the control siRNA and *FBXW7* siRNA groups. The level of *FBXW7* mRNA was substantially reduced by 70% in *FBXW7* siRNA1 (Fig. 4*A*).

Western blot analysis confirmed expression of c-Myc and cyclin E proteins degradation targets of *FBXW7* in control siRNA and *FBXW7* siRNA groups. The expression levels of c-Myc and cyclin E protein were enhanced in the *FBXW7* siRNA group compared with the control siRNA group. Likewise, p53 expression was enhanced (Fig. 4*B*). Evaluation of proliferation potency in the *FBXW7* siRNA groups using the 3-(4,5-dimethylthiazol-2-yl)-2,5-diphenyltetrazolium bromide assay showed that proliferation rates were significantly enhanced in both *FBXW7* groups in comparison with the control siRNA group and parent cell line AZ521 (Fig. 4*C*).

***p53* mutation and *FBXW7* expression are associated with poor prognosis in clinical gastric cancer patients.** *FBXW7* mRNA expression was inhibited in *p53* mutation (+) gastric cancer tissues, and the low *FBXW7* expression patients had a significantly poorer prognosis than the high *FBXW7* expression patients (Figs. 1*B* and 3).

Therefore, we divided 81 gastric cancer patients into four groups according to *FBXW7* expression level and the state of the *p53* mutation and examined the overall survival curve in these groups. The *p53* mutation (+), *FBXW7* low expression group (n = 24) had a significantly poorer prognosis than the other three groups (P = 0.0033; Fig. 5).

Discussion

In this study, we showed that *FBXW7* mRNA expression in gastric cancer samples is markedly decreased in comparison with the corresponding noncancerous samples and that *FBXW7* is a poor prognostic factor. There are three possible explanations. First, it is worth noting that *FBXW7* expression is regulated by p53 in *in vitro* and *in vivo* experimental data (3, 5, 6, 19). For instance, Mao and colleagues reported that *Fbxw7* mRNA expression was activated when *p53* expression was induced by radiation, and baseline expression of *Fbxw7* mRNA is suppressed in $p53^{-/-}$ mice. Moreover, they reported that a p53-binding site is present in a promoter region of the mouse *Fbxw7* (3). In addition, Kimura and colleagues reported that *FBXW7* β expression is enhanced when wild-type *p53* is produced in a *p53*-mutated glioblastoma cell line (8). These reports strongly suggest that transcription of *FBXW7* is regulated by p53 activity. Therefore, we focused on the regulation of *FBXW7* expression by p53 in gastric cancer cases. In the current study, *FBXW7* expression levels were decreased in most *p53* mutation (+) gastric cancer samples (Fig. 3); only 6% (5 of 81) cases were *FBXW7* high expression in *p53* mutation (+; Fig. 5). Most of the p53 mutation (+) gastric cancer patients belonged to the *FBXW7* low expression group. Therefore, we propose that *FBXW7* mRNA expression is primarily regulated by the presence of the *p53* mutation in clinical gastric cancer cases. It is worth noting that the reproducibility of this finding *in vivo* was clearly confirmed in human clinical cases. To determine which isoform of *FBXW7* is regulated by p53 *in vitro*, we used *p53* siRNA to suppress *p53* expression in gastric cancer cell line AZ521. The expression levels of the three *FBXW7* isoforms (α, β, and γ) were suppressed by *p53* siRNA (Supplementary Fig. S6).

Second, we determined that *FBXW7* is inactivated by a mutation in the coding region. The average of *FBXW7* mutation rate in several malignancies was ~6% (4). As for gastric cancer cases, Lee and colleagues reported the possibility of the presence of mutation, but the relationship of the *FBXW7* mutation and prognosis was not elucidated (13). Therefore, we examined the sequence of the *FBXW7* isoforms. The *FBXW7* mutation rate, 8.8% (7 of 80), was similar to the 3.7% to 6% previously reported for gastric cancer (4, 13). Mutation hotspots are located in T-cell acute lymphocytic leukemia; however, they were not detected in the current study (13, 20, 21).

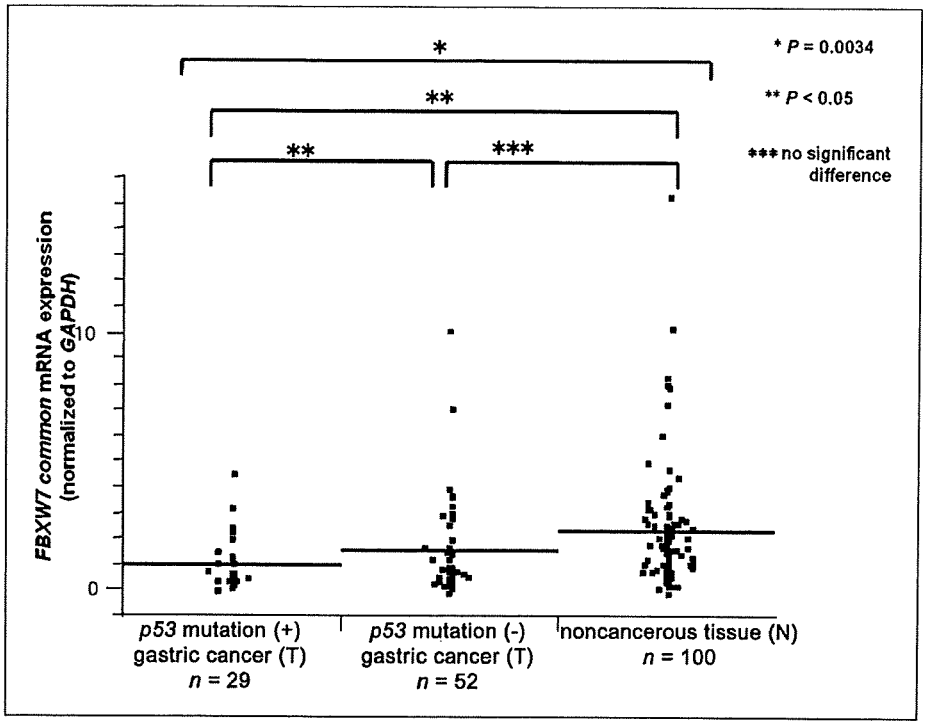

Figure 3. Relationship between *FBXW7* mRNA expression and *p53* mutation. Gastric cancer patients were divided into two groups based on the presence or absence of the *p53* mutation. The two groups were the *p53* mutation (+) gastric cancer group (n = 29) and the *p53* mutation (−) gastric cancer group (n = 52). *FBXW7* expression levels in *p53* mutation (+) patients were lower than in the other groups. *Horizontal lines*, mean expression value of each group. The statistical analysis for comparisons was done in the order of ANOVA and Tukey's test.

Third, chromosome 4q contains the *FBXW7* gene. Approximately 30% of the gene is deleted in certain carcinomas, such as esophageal and gastric cancers. In particular, inactivation of tumor suppressor genes by the chromosome 4q deletion may be an important factor in colon carcinogenesis (22–24).

The reduction of *FBXW7* expression is associated with the dysregulation of cyclin E and c-Myc, positive regulators of the cell cycle (2, 18, 25, 26). c-Myc is associated with cell growth and is recognized as an important factor in control of the G_1 (G_0) to S-phase transition (1, 6, 27, 28). Cyclin E expression is enhanced in various types of cancer, where it regulates cell cycle progression via Rb phosphorylation and contributes to genome instability (19, 29). Consistent with previously published reports, we showed that protein expression of c-Myc and cyclin E is enhanced when *FBXW7* is suppressed in a gastric cancer cell line (Fig. 4). Immunohistochemical analysis of FBXW7 in clinical gastric cancer tissues revealed enhanced expression of Myc and cyclin E in FBXW7 low expression tissues (Supplementary Fig. S7*A*). Conversely, Myc and

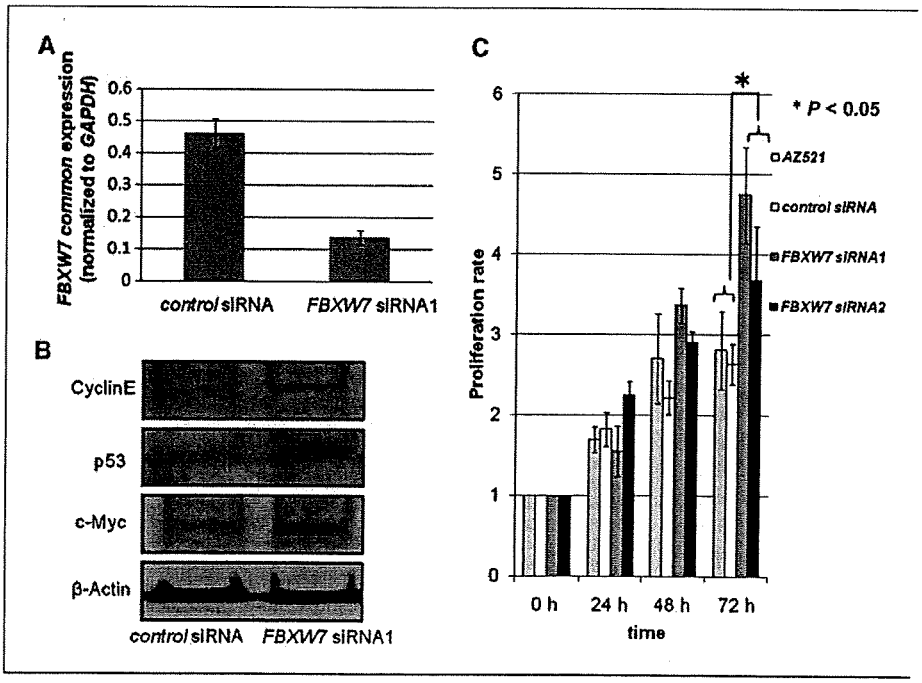

Figure 4. Proliferation assay with RNA interference of *FBXW7* in the AZ521 gastric cancer cell line. *A*, reduced *FBXW7* expression was confirmed by quantitative reverse transcription-PCR analyses in *FBXW7* siRNA1 cells compared with control siRNA. *FBXW7* expressions were normalized by *GAPDH* expression. Mean ± SD. *B*, Western blot analysis of c-Myc, cyclin E, and p53 in *FBXW7* siRNA cells and control siRNA cells. These proteins were normalized to the level of β-actin. *C*, 3-(4,5-dimethylthiazol-2-yl)-2,5-diphenyltetrazolium bromide assay. The proliferation rate of *FBXW7* siRNA (1 and 2) cells was enhanced over that of control siRNA and parent AZ521 cells. Mean ± SD.

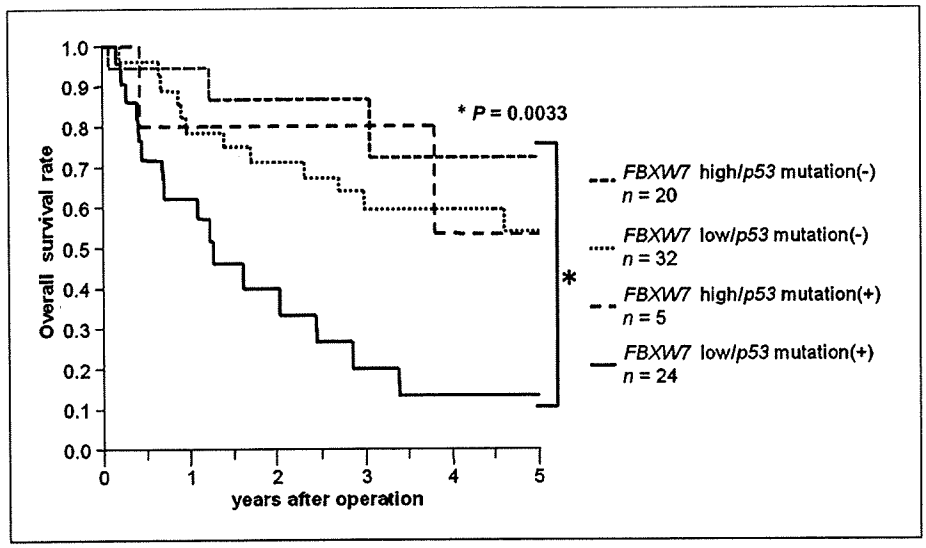

Figure 5. Kaplan-Meier overall survival curves of gastric cancer patients based on *FBXW7* mRNA expression and *p53* mutation. The survival rate for patients in the low *FBXW7* expression and *p53* mutation (+) group was significantly lower than that for patients in the other three groups ($P < 0.05$): high *FBXW7* expression and *p53* mutation (−; $n = 20$), high *FBXW7* expression and *p53* mutation (+; $n = 5$), low *FBXW7* expression and *p53* mutation (−; $n = 32$), and low *FBXW7* expression and *p53* mutation (+; $n = 24$).

cyclin E expression levels were suppressed in tissues in which FBXW7 was overexpressed (Supplementary Fig. S7*B*), confirming the relationship between FBXW7 and target proteins in clinical gastric cancer tissues.

In addition, c-Myc accumulation induces p53-dependent apoptosis via MDM2 degradation (6, 30, 31). The inactivation of both *FBXW7* and *p53* promotes c-Myc accumulation and inhibits p53-dependent apoptosis by MDM2 activation. It probably means that the proliferation rate was increased in these cells.

The low *FBXW7* expression group of gastric cancer patients showed progression of clinicopathologic factors and poor prognosis. All 4 cases of liver metastasis (100%, 4 of 4), 16 cases of peritoneal dissemination (94%, 16 of 17), and 24 cases of venous invasion (86%, 24 of 28) were classified as members of the *FBXW7* low expression group (Table 1). Unfortunately, a significant correlation was not observed between the incidence of liver metastasis and *FBXW7* expression because of an insufficient number of cases. However, other clinicopathologic findings indicated that FBXW7 contributes to hematogenous metastasis besides lymph node metastasis and peritoneal dissemination.

FBXW7 is a tumor suppressor. Considering tumor dormancy as one way to conquer malignancies, the introduction of FBXW7 may facilitate "tumor dormancy therapy." Moreover, it was found that Myc inhibition triggers rapid regression of incipient and established lung tumors *in vivo* (32). Therefore, Myc degradation by FBXW7 may not only induce a state of tumor dormancy but also could have an antitumor effect.

As in a previous *in vivo* study, the simultaneous disruption of two cell cycle checkpoint genes, *p53* and *FBXW7*, shortened the survival of mice with thymic lymphomas (6). It is notable that, even in the *FBXW7* low expression group, the 5-year survival rate of *p53* mutation (−) cases is 53%, but we found that it was 14% in the *FBXW7* low expression/*p53* mutation (+) group of clinical gastric cancer patients (Fig. 5). Both *p53* and *FBXW7* act to brake the cell cycle. Therefore, simultaneous disruption of these genes led to poor prognosis in clinical gastric cancer in comparison with inactivation of *p53* or *FBXW7* alone. Although p53 reportedly regulates *FBXW7* expression, other mechanisms may be present. In the current study, most cases of *p53* mutation (+) gastric cancer were in the low *FBXW7* group and had poor prognosis (83%, 24 of 29). However, a few cases of *p53* mutation (+) gastric cancer were in the high *FBXW7* expression group (17%, 5 of 29) and had good prognosis in comparison with the *p53* mutation (+)/low *FBXW7* group. There were a few cancer cases with higher *FBXW7* expression that was not regulated by p53. Therefore, the prognosis of *p53* mutation (+) cases is not identical to that of *p53* mutation (+)/*FBXW7* low cases.

These results show that the status of *FBXW7* and *p53* is critical for prognosis determination in gastric cancer patients. This report is the first confirmation of the experimental mice data using clinical gastric cancer samples.

In conclusion, *FBXW7* has recently attracted attention as a tumor suppressor gene that reduces important oncoproteins and related carcinogenesis and cell cycle progression. There are previous reports of *in vitro* and *in vivo* studies showing that p53 controls *FBXW7* expression and that *FBXW7* inactivation contributes to poor prognosis via genome instability and cell cycle progression. However, these findings had not been shown in clinical cancer samples. We have clarified that gastric cancer patients with inactivation of *FBXW7* and *p53* have a poorer prognosis.

Disclosure of Potential Conflicts of Interest

No potential conflicts of interest were disclosed.

Acknowledgments

Received 8/5/08; revised 2/2/09; accepted 2/25/09; published OnlineFirst 4/14/09.

Grant support: CREST, Japan Science and Technology Agency; Japan Society for the Promotion of Science Grant-in-Aid for Scientific Research grants 17109013, 18659384, 18390367, 18590333, 18015039, 19591509, 19390336, 20390360, 20591547, 20790961, 20659209, and 20790960; The Ministry of Education, Culture, Sports, Science and Technology Grant-in-Aid for Scientific Research on Priority Areas grant 18015039; Third-Term Comprehensive 10-Year Strategy for Cancer Control grant 16271201; New Energy and Industrial Technology Development Organization Technological Development for Chromosome Analysis; The Ministry of Education, Culture, Sports, Science and Technology of Japan for Scientific Research on Priority Areas, Cancer Translational Research Project; and Grant of Clinical Research Foundation 2008-2010.

The costs of publication of this article were defrayed in part by the payment of page charges. This article must therefore be hereby marked *advertisement* in accordance with 18 U.S.C. Section 1734 solely to indicate this fact.

We thank T. Shimooka, K. Ogata, M. Kasagi, Y. Nakagawa, and T. Kawano for technical assistance.

References

1. Nakayama KI, Nakayama K. Ubiquitin ligases: cell-cycle control and cancer. Nat Rev Cancer 2006;6:369–81.
2. Welcker M, Clurman BE. FBW7 ubiquitin ligase: a tumour suppressor at the crossroads of cell division, growth and differentiation. Nat Rev Cancer 2008;8:83–93.
3. Mao JH, Perez-Losada J, Wu D, et al. Fbxw7/Cdc4 is a p53-dependent, haploinsufficient tumour suppressor gene. Nature 2004;432:775–9.
4. Akhoondi S, Sun D, von der Lehr N, et al. FBXW7/hCDC4 is a general tumor suppressor in human cancer. Cancer Res 2007;67:9006–12.
5. Matsumoto A, Onoyama I, Nakayama KI. Expression of mouse Fbxw7 isoforms is regulated in a cell cycle- or p53-dependent manner. Biochem Biophys Res Commun 2006;350:114–9.
6. Onoyama I, Tsunematsu R, Matsumoto A, et al. Conditional inactivation of Fbxw7 impairs cell-cycle exit during T cell differentiation and results in lymphomatogenesis. J Exp Med 2007;204:2875–88.
7. Matsuoka S, Oike Y, Onoyama I, et al. Fbxw7 acts as a critical fail-safe against premature loss of hematopoietic stem cells and development of T-ALL. Genes Dev 2008;22:986–91.
8. Kimura T, Gotoh M, Nakamura Y, Arakawa H. hCDC4b, a regulator of cyclin E, as a direct transcriptional target of p53. Cancer Sci 2003;94:431–6.
9. Nakayama KI, Nakayama K. Regulation of the cell cycle by SCF-type ubiquitin ligases. Semin Cell Dev Biol 2005;16:323–33.
10. Yan T, Wunder JS, Gokgoz N, Seto KK, Bell RS, Andrulis IL. hCDC4 variation in osteosarcoma. Cancer Genet Cytogenet 2006;169:138–42.
11. Hagedorn M, Delugin M, Abraldes I, et al. FBXW7/hCDC4 controls glioma cell proliferation *in vitro* and is a prognostic marker for survival in glioblastoma patients. Cell Div 2007;2:9.
12. Bredel M, Bredel C, Juric D, et al. Functional network analysis reveals extended gliomagenesis pathway maps and three novel MYC-interacting genes in human gliomas. Cancer Res 2005;65:8679–89.
13. Lee JW, Soung YH, Kim HJ, et al. Mutational analysis of the hCDC4 gene in gastric carcinomas. Eur J Cancer 2006;42:2369–73.
14. Enders GH. Cyclins in breast cancer: too much of a good thing. Breast Cancer Res 2002;4:145–7.
15. Ogawa K, Utsunomiya T, Mimori K, et al. Clinical significance of human kallikrein gene 6 messenger RNA expression in colorectal cancer. Clin Cancer Res 2005;11:2889–93.
16. Ieta K, Ojima E, Tanaka F, et al. Identification of overexpressed genes in hepatocellular carcinoma, with special reference to ubiquitin-conjugating enzyme E2C gene expression. Int J Cancer 2007;121:33–8.
17. Ieta K, Tanaka F, Utsunomiya T, Kuwano H, Mori M. CEACAM6 gene expression in intrahepatic cholangiocarcinoma. Br J Cancer 2006;95:532–40.
18. Welcker M, Orian A, Grim JE, Eisenman RN, Clurman BE. A nucleolar isoform of the Fbw7 ubiquitin ligase regulates c-Myc and cell size. Curr Biol 2004;14:1852–7.
19. Minella AC, Grim JE, Welcker M, Clurman BE. p53 and SCF(Fbw7) cooperatively restrain cyclin E-associated genome instability. Oncogene 2007;26:6948–53.
20. Malyukova A, Dohda T, von der Lehr N, et al. The tumor suppressor gene hCDC4 is frequently mutated in human T-cell acute lymphoblastic leukemia with functional consequences for Notch signaling. Cancer Res 2007;67:5611–6.
21. Tan Y, Sangfelt O, Spruck C. The Fbxw7/hCdc4 tumor suppressor in human cancer. Cancer Lett 2008;271:1–12.
22. Sterian A, Kan T, Berki AT, et al. Mutational and LOH analyses of the chromosome 4q region in esophageal adenocarcinoma. Oncology 2006;70:168–72.
23. Sundqvist A, Bengoechea-Alonso MT, Ye X, et al. Control of lipid metabolism by phosphorylation-dependent degradation of the SREBP family of transcription factors by SCF(Fbw7). Cell Metab 2005;1:379–91.
24. Takada H, Imoto I, Tsuda H, et al. Screening of DNA copy-number aberrations in gastric cancer cell lines by array-based comparative genomic hybridization. Cancer Sci 2005;96:100–10.
25. Welcker M, Orian A, Jin J, et al. The Fbw7 tumor suppressor regulates glycogen synthase kinase 3 phosphorylation-dependent c-Myc protein degradation. Proc Natl Acad Sci U S A 2004;101:9085–90.
26. Welcker M, Singer J, Loeb KR, et al. Multisite phosphorylation by Cdk2 and GSK3 controls cyclin E degradation. Mol Cell 2003;12:381–92.
27. Spencer CA, Groudine M. Control of c-myc regulation in normal and neoplastic cells. Adv Cancer Res 1991;56:1–48.
28. Onoyama I. Cyclin E and c-Myc degradation by SCF(Fbxw7). Tanpakushitsu Kakusan Koso 2006;51:1382–5.
29. Ji P, Zhu L. Using kinetic studies to uncover new Rb functions in inhibiting cell cycle progression. Cell Cycle 2005;4:373–5.
30. Zindy F, Eischen CM, Randle DH, et al. Myc signaling via the ARF tumor suppressor regulates p53-dependent apoptosis and immortalization. Genes Dev 1998;12:2424–33.
31. Pelengaris S, Khan M. The many faces of c-MYC. Arch Biochem Biophys 2003;416:129–36.
32. Soucek L, Whitfield J, Martins CP, et al. Modelling Myc inhibition as a cancer therapy. Nature 2008;455:679–83.

Hes1 immortalizes committed progenitors and plays a role in blast crisis transition in chronic myelogenous leukemia

Fumio Nakahara,[1-4] Mamiko Sakata-Yanagimoto,[1,2,5] Yukiko Komeno,[3,4] Naoko Kato,[3,4] Tomoyuki Uchida,[3,4] Kyoko Haraguchi,[1,6] Keiki Kumano,[1,2] Yuka Harada,[7] Hironori Harada,[8] Jiro Kitaura,[3,4] Seishi Ogawa,[9] Mineo Kurokawa,[1,2] Toshio Kitamura,[3,4] and Shigeru Chiba[1,5]

[1]Department of Cell Therapy and Transplantation Medicine and [2]Department of Hematology Oncology, University of Tokyo, Tokyo; [3]Division of Cellular Therapy, Advanced Clinical Research Center, University of Tokyo, Tokyo; [4]Division of Stem Cell Signaling, Center for Stem Cell Therapy, Institute of Medical Science, University of Tokyo, Tokyo; [5]Department of Clinical and Experimental Hematology, Graduate School of Comprehensive Human Sciences, University of Tsukuba, Ibaraki; [6]Division of Transfusion and Cell Therapy, Tokyo Metropolitan Cancer and Infectious Disease Center Komagome Hospital, Tokyo; [7]International Radiation Information Center, Hiroshima University, Hiroshima; [8]Department of Hematology and Oncology, Research Institute for Radiation Biology and Medicine, Hiroshima University, Hiroshima; and [9]Cancer Genomics Project, Graduate School of Medicine, University of Tokyo, Tokyo, Japan

Hairy enhancer of split 1 (Hes1) is a basic helix-loop-helix transcriptional repressor that affects differentiation and often helps maintain cells in an immature state in various tissues. Here we show that retroviral expression of Hes1 immortalizes common myeloid progenitors (CMPs) and granulocyte-macrophage progenitors (GMPs) in the presence of interleukin-3, conferring permanent replating capability on these cells. Whereas these cells did not develop myeloproliferative neoplasms when intravenously administered to irradiated mice, the combination of Hes1 and BCR-ABL in CMPs and GMPs caused acute leukemia resembling blast crisis of chronic myelogenous leukemia (CML), resulting in rapid death of the recipient mice. On the other hand, BCR-ABL alone caused CML-like disease when expressed in c-Kit-positive, Sca-1-positive, and lineage-negative hematopoietic stem cells (KSLs), but not committed progenitors CMPs or GMPs, as previously reported. Leukemic cells derived from Hes1 and BCR-ABL-expressing CMPs and GMPs were more immature than those derived from BCR-ABL-expressing KSLs. Intriguingly, Hes1 was highly expressed in 8 of 20 patients with CML in blast crisis, but not in the chronic phase, and dominant negative Hes1 retarded the growth of some CML cell lines expressing Hes1. These results suggest that Hes1 is a key molecule in blast crisis transition in CML. (*Blood.* 2010;115(14):2872-2881)

Introduction

The balance between activator and repressor basic helix-loop-helix transcription factors is crucial for the proper timing of cellular differentiation and normal morphogenesis of various tissues.[1] During embryogenesis, the basic helix-loop-helix protein hairy enhancer of split 1 (Hes1), functioning downstream of the Notch receptor,[2,3] blocks differentiation of neural stem cells by antagonizing Mash1[4] and affects the cell-fate decision of pancreatobiliary epithelial progenitors.[5] In the adult hematopoietic system, Hes1 blocks granulocyte colony-stimulating factor-induced granulocytic differentiation of the 32D cell line,[6] preserving the long-term reconstituting ability of hematopoietic stem cells (HSCs) in vitro as well as in vivo.[7] Hes1 also plays a significant role in the development of perinatal T cells,[8,9] and knocking out Hes1 leads to lack of thymus.[9]

Recently, activating mutations of the *Notch1* and *Notch2* genes have been identified in more than 50% of human T-cell acute lymphoblastic leukemias[10] and in a subset of non-Hodgkin lymphomas,[11] respectively, implicating Notch signal deregulation based on a genetic abnormality in human cancers. The effect of Notch signal aberration, however, has been largely confined to lymphoid lineages in the hematopoietic compartment. Indeed, enhanced Notch signaling provides the bone-marrow-to-thymus transition stage of early progenitors, with strong selective pressure toward thymic T-cell precursors at the expense of B-cell and myeloid precursors.[12-14] We recently found that up-regulation of Hes1 represents only a part of Notch signaling during the decision between mast cell and granulocyte lineage differentiation. Notch signaling does promote mast-cell development at the expense of granulocyte differentiation through up-regulation of both Hes1 and GATA-3 in common myeloid progenitors (CMPs) and granulocyte-macrophage progenitors (GMPs). However, up-regulation of Hes1 alone causes expansion of cells with myeloid progenitor phenotypes, rather than mast cell development, mediated through down-regulation of a transcription factor, C-enhancer binding protein α (C/EBP-α).[15]

A growing volume of evidence shows that down-regulation of C/EBP-α represents major events in human acute myelogenous leukemia (AML), through either genetic or epigenetic abnormalities. Therefore, it is postulated that Hes1 up-regulation may be involved in a subset of myeloid leukemias.

Chronic myelogenous leukemia (CML) is a myeloproliferative neoplasm that originates in an abnormal pluripotent bone marrow stem cell and is consistently associated with the *BCR-ABL* fusion gene. The disease is biphasic or triphasic; an initial indolent chronic phase is followed by one or both of the aggressive stages, the accelerated phase and blast crisis, resulting in expansion of immature leukemic cells. The mainstay of chronic phase to blast

Submitted May 19, 2009; accepted September 27, 2009. Prepublished online as *Blood* First Edition paper, October 27, 2009; DOI 10.1182/blood-2009-05-222836.

The online version of this article contains a data supplement.

The publication costs of this article were defrayed in part by page charge payment. Therefore, and solely to indicate this fact, this article is hereby marked "advertisement" in accordance with 18 USC section 1734.

crisis transition is the differentiation block by additional genetic events in progenitor stages of CML cells[16] that could otherwise differentiate during the chronic phase. Thus, the transformation of BCR-ABL-induced myeloproliferative neoplasm to full-blown blast crisis has been drawing tremendous attention from investigators.

Here we show that retroviral expression of Hes1 immortalizes CMPs and GMPs in vitro. Hes1 introduction together with BCR-ABL into CMPs and GMPs, the postulated origin of blast crisis transition in CML, induced CML blast crisis-like disease when intravenously administered to sublethally irradiated mice. Considering as well the study of Hes1 expression in CML patients, we propose that Hes1 is a unique experimental tool for studying the mechanisms of chronic phase to blast crisis transformation in CML.

Methods

Mice

C57BL/6 (Ly5.1) donor mice were purchased from Sankyo Labo Service Corporation. C57BL/6 (Ly5.2) recipient mice were purchased from SLC. Mice were kept at the Animal Center for Biomedical Research, University of Tokyo, according to institutional guidelines.

Bone marrow progenitor sort

Bone marrow cells were isolated from the femurs and tibias of C57BL/6 (Ly5.1) donor mice (8-10 weeks of age) and were incubated with biotinylated antibodies for lineage markers, including anti-CD3, anti-CD4, anti-CD8, anti-B220, anti-Ter119, and anti–Gr-1 antibodies (BD Biosciences PharMingen) followed by incubation with streptavidin Micro Beads (Miltenyi Biotec). The lineage marker-negative (Lin^-) fraction was separated with an autoMACS separator or LS Columns (Miltenyi Biotec) and incubated with anti-CD34–fluorescein isothiocyanate, anti-CD16/32 (FcγRIII/II receptor)–phycoerythrin (PE), anti–c-Kit–allophycocyanin, streptavidin peridinin chlorophyll protein (BD Biosciences PharMingen), and anti–Sca-1–PE/Cy7 (eBioscience). $Lin^-c\text{-}Kit^+Sca\text{-}1^+$, $Lin^-c\text{-}Kit^+Sca\text{-}1^-Fc\gamma R^{lo}CD34^+$, and $Lin^-c\text{-}Kit^+Sca\text{-}1^-Fc\gamma R^{hi}CD34^+$ cells (KSLs, CMPs, and GMPs, respectively)[17] were sorted with a FACSAria cell sorter (BD Biosciences).

Transfection and retrovirus production for murine cells

Rat Hes1 cDNA, a gift from R. Kageyama (Kyoto University, Kyoto, Japan), was subcloned into a retrovirus vector, GCDNsam/internal ribosome entry site (IRES)–nerve growth factor receptor (NGFR), a gift from H. Nakauchi (University of Tokyo) and M. Onodera (National Center for Child Health and Development, Tokyo, Japan). BCR-ABL (p210) cDNA[18] was subcloned into a retrovirus vector, GCDNsam/IRES-GFP.[19] Mouse C/EBP-α cDNA, a gift from K. Akashi (Kyushu University, Fukuoka, Japan) and S. Mizuno (Dana-Farber Cancer Institute, Boston, MA), was subcloned into a retrovirus vector, pMYs-IRES-GFP.[19] Plat-E[20] packaging cells maintained in Dulbecco modified Eagle medium supplemented with 10% fetal calf serum were transfected with retroviral constructs using FuGENE 6 transfection reagent (Roche Diagnostics) according to the manufacturer's instructions. The medium was changed a day after transfection, and retroviruses were harvested 48 hours after transfection, as previously described.[19,20]

Transfection and retrovirus production for human cell lines

We generated a dominant-negative Hes1 (dnHes1) lacking a C-terminal WRPW (Trp-Arg-Pro-Trp) domain as described.[21] The fragment of dnHes1 was subcloned into pMYs-IRES-GFP.[19] Retrovirus packaging was done as described. Briefly, retroviruses were generated by transient transfection of Plat-A[20] packaging cells with FuGENE 6 (Roche Diagnostics).

Infection to progenitors

The retrovirus medium was placed in 24-well nontissue culture dishes for 4 hours at 37°C, precoated with 40 μg/mL of RetroNectin (Takara Bio) overnight at 4°C. After washing the wells with phosphate-buffered saline, sorted KSLs, CMPs, or GMPs were plated for infection for 48 to 60 hours with the coated retroviruses harboring GCDNsam/IRES-GFP-BCR-ABL (p210) or GCDNsam/IRES-NGFR-Hes1 or an empty vector as a control. Infection was done in StemSpan SFEM medium (StemCell Technologies) containing 100 ng/mL mouse stem cell factor (SCF), 100 ng/mL mouse thrombopoietin (TPO), and 100 ng/mL human FLT3 ligand (FL) for KSLs, or in Iscove modified Dulbecco medium (Sigma-Aldrich) containing 20% fetal calf serum, 50 ng/mL mouse SCF, 20 ng/mL mouse TPO, and 20 ng/mL mouse interleukin-3 (IL-3), 20 ng/mL human IL-6 (R&D Systems) for CMPs or GMPs.

Colony-forming assay

Retrovirus-infected cells were sorted at 48 to 60 hours from the initiation of infection with a FACSAria cell sorter (BD Biosciences) and used for colony-forming assay using Methocult 3231 (StemCell Technologies), supplemented with 50 ng/mL mouse SCF, 20 ng/mL mouse TPO, and 20 ng/mL mouse IL-3, 20 ng/mL human IL-6. A total of 1000 cells were cultured in each 2.5-cm dish in duplicate. The colony-forming cells were harvested and replated every 7 to 9 days and scored for colony formation. We defined a colony as "a group of cells, grown from a single parent cell, which is composed of more than 40 live cells."

Mouse bone marrow transplantation

Bone marrow cells prepared from C57BL/6-Ly5.1 mice were infected with retrovirus containing Hes1 or BCR-ABL, and 0.1 to 2.6×10^5 of Hes1/NGFR-sorted or BCR-ABL/GFP-sorted cells were injected through tail veins into C57BL/6-Ly5.2-recipient mice (8-12 weeks of age) after sublethal (5.25 Gy) or lethal (9.5 Gy) total body γ-irradiation (^{135}Cs). For the lethally irradiated mice, 2×10^5 of C57BL/6-Ly5.2 mice-derived bone marrow cells were simultaneously injected for radioprotection. Probabilities of overall survival of the mice that received transplantations were estimated using the Kaplan-Meier method. Statistical differences were determined by the Wilcoxon test. All animal studies were approved by the Animal Care Committee of the Institute of Medical Science, University of Tokyo.

Analysis of mice receiving transplantation

After transplantation, mice were monitored for signs of disease, such as cachexia, hyperpnea, or loss of gloss in fur. Autopsies were performed on moribund recipient mice. Peripheral blood count was analyzed by KX-21 Auto Analyzer (Sysmex). Morphology of the peripheral blood was evaluated by staining of air-dried smears with Hemacolor (Merck). Tissues including bone marrow, spleen, and liver were fixed in 10% buffered formalin, embedded in paraffin, sectioned, and stained with hematoxylin and eosin. Cytospin preparations of bone marrow and spleen cells were also stained with Hemacolor. Percentage of blasts, myelocytes, neutrophils, monocytes, lymphocytes, and erythroblasts was estimated by examination of at least 200 cells. To assess whether the leukemic cells were transplantable to secondary recipients, 0.1 to 5×10^6 total bone marrow cells were injected into the tail veins of sublethally irradiated mice. Two recipient mice were used for each serial transplantation.

Flow cytometric analysis

Red blood cells were lysed using Red Blood Cell Lysing Buffer (Sigma-Aldrich) in peripheral blood or single-cell suspensions of bone marrow and spleen. After washing with phosphate-buffered saline, Fc receptor was blocked by incubating cells with 2.4G2 antibody (eBioscience) for 15 minutes at 4°C and then staining them with the following PE-conjugated monoclonal antibodies for 20 minutes at 4°C: Ly-5.1, Gr-1, CD11b, B220, CD19, CD3, CD4, CD8, c-Kit, Sca-1, CD34, and Ter119. Flow-cytometric analysis of the stained cells was performed with FACSCalibur

(BD Biosciences) equipped with CellQuest software (BD Biosciences) and FlowJo software (TreeStar).

Patients

CML patients were diagnosed at Hiroshima University Hospital and its affiliated hospitals. Diagnosis was based on morphologic, immunophenotypic, and, in some cases, real-time reverse transcription-polymerase chain reaction (RT-PCR) studies according to the French-American-British classification or World Health Organization classification. Patient samples were prepared after the research plan was approved by the Institutional Review Board at Hiroshima University, and written informed consent was obtained in accordance with the Declaration of Helsinki. Investigations were carried out in accordance with ethical standards authorized by the ethics committee of Hiroshima University and the ethics committee of the University of Tokyo (approval no. 20-10-0620)

Real-time RT-PCR

Total RNA was extracted from human bone marrow or peripheral blood cells using a TRIzol Kit (Invitrogen) according to the manufacturer's instructions, and converted to cDNA with a High Capacity cDNA Reverse Transcription Kit (Applied Biosystems). Total RNA of mouse progenitors was extracted with RNeasy (QIAGEN) according to the manufacturer's instructions, and converted to cDNA with a High Capacity cDNA Reverse Transcription Kit (Applied Biosystems). Real-time RT-PCR was performed using a LightCycler Workflow System (Roche Diagnostics). cDNA was amplified using a SYBR Premix EX Taq (Takara). Reaction was subjected to 1 cycle of 95°C for 30 seconds, 45 cycles of PCR at 95°C for 5 seconds, 58°C for 10 seconds, and 72°C for 10 seconds. All samples were independently analyzed at least 3 times. The following primer pairs were used: 5′-CCAGTTTGCTTTCCTCATTCC-3′ (forward) and 5′-TCTTCTCTCCCAGTATTCAAGTTCC-3′ (reverse) for human Hes1[22]; 5′-GAGCTGAACGGGAAGCTCACTGG-3′ (forward) and 5′-CAACTGTGAGGAGGGGAGATTCAG-3′ (reverse) for human GAPDH[22]; 5′-GAACAGCAACGAGTACCGGGTA-3′ (forward) and 5′-CCCATGGCCTTGACCAAGGAG-3′ (reverse) for mouse C/EBP-α[23]; 5′-CACAGGACTAGAACACCTGC-3′ (forward) and 5′-GCTGGTGAAAAGGACCTCT-3′ (reverse) for mouse hypoxanthine phosphoribosyltransferase (HPRT).[23] Relative gene expression levels were calculated using standard curves generated by serial dilutions of cDNA. Product quality was checked by melting curve analysis via LightCycler software (Roche Diagnostics). Expression levels were normalized by a control, the expression level of GAPDH mRNA for human samples, and HPRT mRNA for mouse samples.

Western blot analysis

To detect the expression of Hes1 or BCR-ABL (p210) proteins, equal numbers of cells from spleen or cell line were lysed, and Western blotting was performed as described with minor modifications.[24] Polyclonal rabbit anti-Hes1 antibody (H-140; Santa Cruz Biotechnology) and polyclonal rabbit anti–c-ABL antibody (K-12; Santa Cruz Biotechnology) were used for Hes1 or BCR-ABL detection, respectively.

Results

Retroviral transduction of Hes1 immortalizes CMPs and GMPs

NGFR-sorted Hes1-transduced KSLs, CMPs, and GMPs similarly generated compact and relatively large colonies, whereas empty vector-transduced KSLs generated a similar number of less large colonies. Empty vector-transduced CMPs and GMPs did not generate colonies (Figure 1A). Cytospin preparations of Hes1-transduced progenitors, stained with Hemacolor (Merck), showed blast-like morphologies, whereas those of empty vector-transduced KSLs contained bands, macrophages, and blasts (Figure 1B). Most of the empty vector-transduced CMPs and GMPs died and few cells remained (Figure 1B). In serial colony-forming assays, both CMPs and GMPs transduced with Hes1 formed colonies after at least 4 rounds of replating, with the plating efficiency more than 15% at the fourth round (Figure 1C). Replating could be reproducibly maintained for more than half a year, implying immortalizing activity of Hes1 (Figure 1D). The Hes1-transduced KSLs, CMPs, and GMPs were dependent on the presence of IL-3, requiring concentrations more than 1 ng/mL (Figure 1E; supplemental Figure 1A-B, available on the *Blood* website; see the Supplemental Materials link at the top of the online article). There was no significant difference between these cells in the dependency on IL-3. The majority of Hes1-transduced cells expressed c-Kit and CD34 at high levels, Sca-1 and CD11b at intermediate levels (Figure 1F, supplemental Figure 2A-B), irrespective of whether they were derived from KSLs, CMPs, or GMPs (supplemental Figure 2E).

The Lin^- cells were further analyzed by adopting 5-color flow cytometry that is used to identify bone marrow KSLs, CMPs, and GMPs. The expression levels of c-Kit, Sca-1, and CD34 were distributed over wide ranges. Approximately 2.5% to 6.4% of all nucleated cells showed a phenotype similar to KSLs, and another 4.8% to 11.6% showed a phenotype similar to GMPs. There were few cells that resembled CMPs (Figure 1G). We sorted the KSL-like cells, CMP-like cells, and GMP-like cells from each Hes1-transduced cell (Hes1-KSLs, Hes1-CMPs, and Hes1-GMPs) and cultured them for a week in methylcellulose. The same analysis by 5-color flow cytometry showed accumulation of GMP-like cells (~ 45.3%-83.5% of all nucleated cells) and moderate accumulation of KSL-like cells (~ 4.3%-23.4% of all nucleated cells) in the cultured cells (supplemental Figure 3A-C).

BCR-ABL replaces IL-3 in Hes1-immortalized cell lines

Because the Hes1-immortalized cell lines were IL-3 dependent for their growth in vitro, we examined whether additional signaling could replace IL-3. IL-3 signaling takes place mainly via Stat-, Ras-MAPK-, and PI3K-Akt-dependent pathways. It is also known that CML-specific BCR-ABL (p210) can replace IL-3 signaling in several experimental designs. Thus, we retrovirally expressed BCR-ABL together with Hes1. The combination of Hes1 and BCR-ABL enabled KSLs, CMPs, and GMPs to form colonies after repeated replating, not only in the presence of cytokines (Figure 2A left panel) but also in the condition free from cytokines (Figure 2A right panel). In contrast, KSLs, but not CMPs or GMPs, formed colonies by BCR-ABL transduction alone only when supplemented with cytokines (Figure 2A left panel), and they did not form any colonies without cytokines (Figure 2A right panel) or after replating with/without cytokines (Figure 2A both panels). In the liquid culture, it was shown that KSLs, CMPs, and GMPs transduced with both Hes1 and BCR-ABL were immortalized without cytokine supplementation (Figure 2B). The colonies made from Hes1- and BCR-ABL-transduced cells showed similar morphology with those from Hes1-transduced cells in the presence of a cytokine cocktail (Figure 2C). Importantly, the morphology of colony-forming cells derived from BCR-ABL-transduced KSLs was much more mature compared with those derived from Hes1- and BCR-ABL-transduced KSLs, CMPs, and GMPs, even in the same cytokine cocktail (Figure 2D). The majority of $Hes1^+$BCR-ABL^+ KSLs as well as $Hes1^+$BCR-ABL^+ CMPs and GMPs expressed CD34 at high levels, whereas they expressed c-Kit, Sca-1, and CD11b at intermediate levels (Figure 2E; supplemental Figure 2C-D), irrespective of whether they were derived from

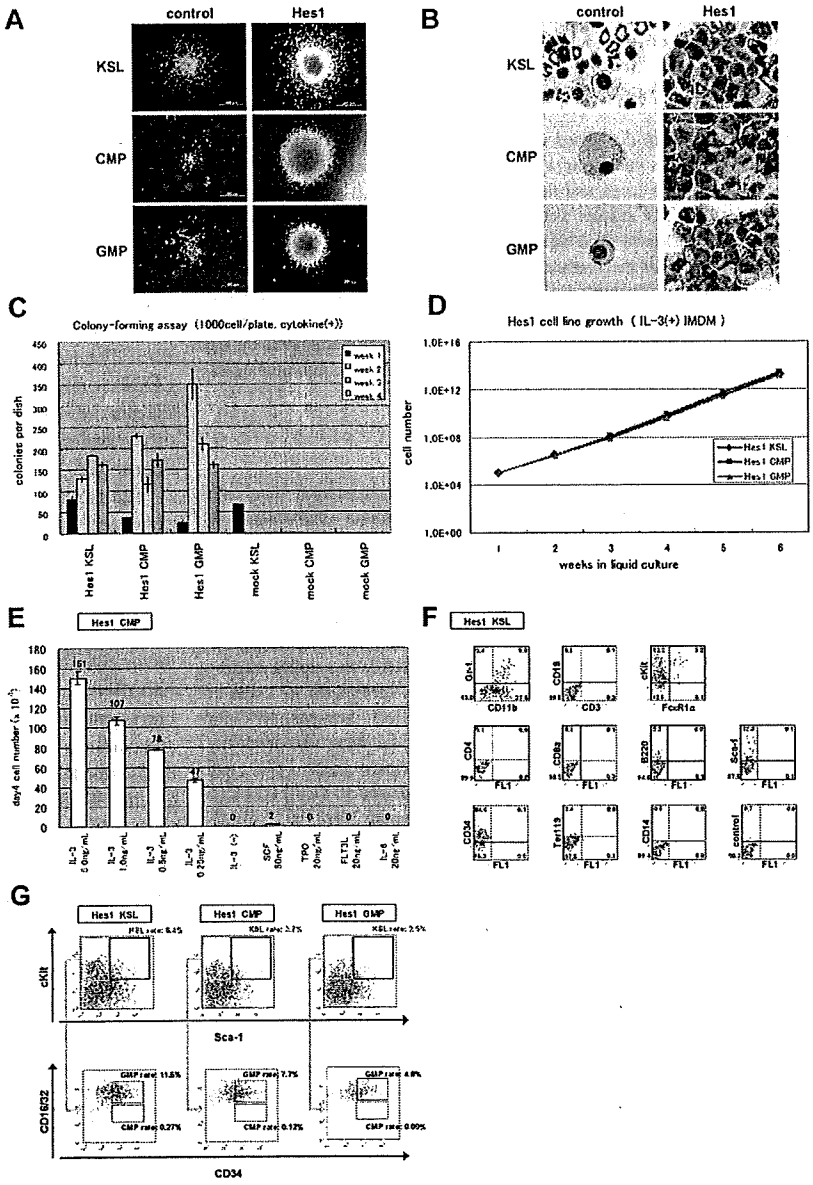

Figure 1. Hes1-transduced KSLs, CMPs, or GMPs were immortalized in the presence of IL-3. (A) Typical colonies derived from Hes1- and empty vector-transduced KSLs, CMPs, and GMPs in the presence of SCF, TPO, IL-3, and IL-6. Images were obtained with an IX70 microscope and a DP70 camera (Olympus); an objective lens, UPlanFI (Olympus); original magnification ×40 (bottom 2 in the right panels) and original magnification ×100 (remaining 4 panels). (B) Giemsa staining of Hes1- and control vector-transduced KSLs, CMPs, and GMPs. Images were obtained with a BX51 microscope and a DP12 camera (Olympus); an objective lens, UPlanFI (Olympus); original magnification ×1000. (C) Colony-forming assay from KSLs, CMPs, and GMPs transduced with Hes1 or empty vector. Hes1-transduced cells were replatable more than 4 times in vitro. Bars represent the number of colonies obtained per 10^3 cells after each round of plating in methylcellulose supplemented with SCF, TPO, IL-3, and IL-6. A representative result from 3 independent and reproducible experiments is shown. Error bars represent the SD from duplicate cultures. (D) Sustained growth of Hes1-transduced cells in liquid culture supplemented with 1 ng/mL IL-3. The number of cells was determined every 7 days by trypan blue staining, and 10^5 cells per well were seeded into a 6-well plate. Liquid culture was reproducibly continued for more than 6 months. (E) Cytokine requirement of Hes1-transduced CMPs. The cells were cultured in Iscove modified Dulbecco medium supplemented with indicated cytokines in duplicate. The numbers of cells were counted after 4 days of culture. A representative result from 2 independent and reproducible experiments is shown. Error bars represent the SD from duplicate cultures. Hes1-transduced KSLs and GMPs showed similar results (supplemental Figure 1A-B). (F) Flow-cytometric analysis of Hes1-transduced KSLs cultured in methylcellulose supplemented with SCF, TPO, IL-3, and IL-6. The dot plots represent Gr-1, CD19, c-Kit, CD4, CD8a, B220, Sca-1, CD34, Ter119, and CD14 labeled with a corresponding PE-conjugated monoclonal antibody versus CD11b, CD3, and FcεR1α labeled with a corresponding fluorescein isothiocyanate-conjugated monoclonal antibody or FL1 with no monoclonal antibody. Hes1-transduced CMPs and GMPs showed similar expression patterns (supplemental Figure 2A-B). (G) Flow-cytometric analysis of Lin$^-$-gated Hes1-transduced cells. Five-color analyses are used to identify KSL-like (top panels) and CMP-like and GMP-like cells (bottom panels) in the Hes1-transduced KSLs, CMPs, and GMPs. The number shows the percentage of cells in all nucleated cells. The analyzed cells were NGFR sorted at 48 to 60 hours from the initiation of Hes1- or control vector-transduction and cultured for the following lengths of time before the analysis: (A) 1 week, (B) 1 week, (C) 0 days, (D) 4 weeks, (E) 2 weeks, (F) 1 week, and (E) 2 weeks.

KSLs, CMPs, or GMPs (supplemental Figure 2F). Hes1$^+$BCR-ABL$^+$ KSLs, CMPs, and GMPs showed lower expressions of c-Kit and CD34 than KSLs, CMPs, and GMPs transduced with Hes1 alone (supplemental Figure 2E-F) when cultured in the presence of the same cytokine cocktail (SCF, TPO, IL-3, and IL-6). Expression of Hes1 or BCR-ABL in the Hes1 ± BCR-ABL transduced CMP or GMP cell lines was confirmed by Western blot analysis (supplemental Figure 4A).

Hes1$^+$BCR-ABL$^+$ CMPs and GMPs rapidly induce AML/CML blast crisis-like disease in recipient mice

To examine the effect of Hes1 on leukemogenesis, Hes1-transduced KSLs, CMPs, and GMPs were injected through tail veins into C57BL/6-Ly5.2 recipient mice (8-12 weeks of age) after a sublethal (5.25 Gy) or a lethal (9.5 Gy) dose of total-body γ-irradiation (^{135}Cs). For the lethally irradiated mice, 2×10^5 bone marrow cells from C57BL/6-Ly5.2 mice were simultaneously injected for radioprotection. All the mice that received transplantations of Hes1-transduced KSLs, CMPs, and GMPs were kept healthy, and no recipients developed myeloproliferative neoplasms (MPNs) or leukemias for up to 250 days after the transplantation (Figure 3A). Regarding the nonleukemogenic nature of the stem/progenitor cells transduced with Hes1 alone, we[7] and others[25] previously reported similar results, although the cell populations and/or experimental designs were not identical.

In agreement with the previous reports,[26] recipient mice injected with BCR-ABL-transduced KSLs developed fatal MPN within 30 days after the transplantation, whereas those injected with BCR-ABL-transduced CMPs and GMPs were kept healthy for more than 130 days. We did not find any signs of MPN or leukemias when mice were killed between 130 and 200 days after the transplantation (Figure 3B).

Because we found that the combination of Hes1 and BCR-ABL transduction conferred cytokine-independent immortalization on CMPs and GMPs, we injected Hes1$^+$BCR-ABL$^+$ KSLs, CMPs, and GMPs through tail veins into C57BL/6-Ly5.2 recipient mice